Spin effects and baryon resonance dynamics in ϕ-meson photoproduction at few GeV

A. I. Titov[1,2] and T.-S. H. Lee[3]
[1]*Advanced Science Research Center, Japan Atomic Energy Research Institute, Tokai, Ibaraki 319-1195, Japan*
[2]*Bogoliubov Laboratory of Theoretical Physics, JINR, Dubna 141980, Russia*
[3]*Physics Division, Argonne National Laboratory, Argonne, Illinois 60439, USA*
(Received 25 December 2002; published 27 June 2003)

The diffractive ϕ-meson photoproduction amplitude is dominated by the Pomeron-exchange process and contains the terms that govern the spin-spin and spin-orbital interactions. We show that these terms are responsible for the spin-flip transitions at forward photoproduction angles and appear in the angular distributions of $\phi \to K^+K^-$ decay in reactions with unpolarized and polarized photon beams. At large momentum transfers, the main contribution to the ϕ-meson photoproduction is found to be due to the excitation of nucleon resonances. Combined analysis of ω and ϕ photoproduction indicates strong Okubo-Zweig-Iizuka–rule violation in ϕNN^* couplings. We also show that the spin observables are sensitive to the dynamics of ϕ-meson photoproduction at large angles and could help to distinguish different theoretical models of nucleon resonances. Predictions for spin effects in ϕ-meson photoproduction are presented for future experimental tests.

DOI: 10.1103/PhysRevC.67.065205 PACS number(s): 13.88.+e, 13.60.Le, 14.20.Gk, 25.20.Lj

I. INTRODUCTION

The photoproduction of light vector meson (ρ, ω, ϕ) is an interesting reaction for many reasons. At high energies ($W \equiv \sqrt{s} \gtrsim 10$ GeV), it brings information on the dynamics of the Pomeron exchange [1–8]. At low energies ($W \sim 2$ GeV), its observables are sensitive to the resonance channel and can be used to obtain some unique information about the structure of baryon resonances, properties of VNN^* interactions [9–16], and possible manifestation of the so-called ''missing resonances'' [17–19]. Therefore, the study of vector-meson photoproductions is an important component of the experimental programs at the electron and photon facilities such as the Thomas Jefferson National Accelerator Facility, the LEPS at SPring-8, the ELSA-SAPHIR at Bonn, and the GRAAL at Grenoble. The ϕ-meson photoproduction at relatively low energies $E_\gamma \simeq 2$–3 GeV plays a particularly important role. It is expected that in the diffractive region, the dominant contribution comes from the Pomeron exchange, since trajectories associated with conventional meson exchanges are suppressed by the OZI rule. The exception is the finite contribution of the pseudoscalar π, η-meson-exchange channel, but its properties are quite well understood [20,21]. Therefore, the low-energy ϕ-meson photoproduction may be used for studying the presence of additional trajectories. Candidates are trajectories associated with a scalar meson [20,22] and f_2' meson [21] containing a large amount of strangeness, glueball [23], or other exotic channels [24]. But the relative contributions of these additional processes cannot be well defined within the Regge phenomenology and must be determined from comparisons with experimental data. Spin observables are of crucial importance for such studies. As a matter of fact, the Pomeron-exchange amplitude which is inspired by multigluon exchange [1] contains specific spin-dependence terms that are negligible in ϕ-meson photoproduction at high energies but become important at a few GeV. These interactions lead to spin-flip processes and give nontrivial behavior of the spin-density matrix elements even at forward angles. Therefore, the angular distribution of $\phi \to K^+K^-$ decay can be used as a tool to study the diffractive mechanism, and is complementary to the measurement of unpolarized cross section.

Another subject is related to the strange degrees of freedom in a nucleon. Analysis of magnetic [25,26] and electroweak [27] moments of baryons show that the ϕ meson couples more strongly to the nucleon than expected on the basis of the Okubo-Zweig-Iizuka (OZI) rule [28]. The presence of the strange-quark content in the nucleon was indicated by measurements of the π-nucleon term [29], ϕ-meson production in proton annihilation at rest [30–32], and deep-inelastic electroweak lepton-nucleon scattering (see Ref. [33] for references and a compilation of the data).

The ϕ-meson photoproduction seems to be an effective and promising candidate process for studying the hidden strangeness in a nucleon. The backward-angle photoproduction is dominated by s and u channels of the nucleon and resonant amplitudes, and directly related to the strength of ϕNN and ϕNN^* interactions. The finite strange content leads to an increase of this strength compared to the expectation based on the standard OZI-rule violation (OZI-rule-evading interaction [22]). This effect must be seen in both unpolarized and spin observables at large momentum transfers.

At forward angles, the nucleon and resonant contributions become negligible for ϕ-meson photoproduction and OZI-rule violation could appear as direct $s\bar{s}$ knockout [34] from a nucleon. Here, the measurement of spin observables that represent the interference of the weak $s\bar{s}$ knockout and strong vector-meson dominance photoproduction amplitudes [35–37] is the most promising feature. It is clear that for this purpose the diffractive amplitude must be established unambiguously.

The purpose of this paper is to investigate the problems mentioned above. The main differences with the previous studies of the conventional nonstrange amplitude of $\gamma p \to \phi p$ reaction [20,22] are in giving a detailed analysis of the

spin properties of the amplitude in the diffractive region. We will present a comprehensive analysis of all spin-density matrix elements which are responsible for the angular distributions of K^+K^- in the reaction $\gamma p \to \phi p$ with unpolarized and polarized photons at a few GeV. For the most important matrix elements we give an estimation in an explicit analytical form, which is useful for the qualitative analysis.

The backward-angle photoproduction is described by the nucleon resonance excitations. For the latter, we use an effective Lagrangian approach developed for ω-meson photoproduction [16], where all known nucleon resonances listed in the Particle Data Group [38] are included. This resonant model is different from the approach of Ref. [14], which results in giving significantly different predictions of some spin observables.

This paper is organized as follows. In Sec. II we define the kinematics and observables. The formula for the calculation of various spin observables are also introduced here. The basic amplitudes for the conventional processes, such as the Pomeron exchange, Reggeon exchanges, and resonance excitations, are given in Sec. III. In Sec. IV we discuss results and make predictions for the future experiments. The summary is given in Sec. V. In the Appendix we discuss an extreme case where the exotic trajectories become dominant in the near-threshold energy region.

II. KINEMATICS AND OBSERVABLES

The scattering amplitude T of the $\gamma p \to Vp$ reaction (where V can be ϕ or ω) is related to the S matrix by

$$S_{fi} = \delta_{fi} - i(2\pi)^4 \delta^4(k+p-q-p') T_{fi}, \tag{1}$$

where k, q, p, and p' denote the four-momenta of the incoming photon, outgoing vector meson, initial nucleon, and final nucleon, respectively. The standard Mandelstam variables are defined by $t=(p-p')^2=(q-k)^2$, $s \equiv W^2=(p+k)^2$, and the vector-meson production angle θ by $\cos\theta \equiv \mathbf{k}\cdot\mathbf{q}/|\mathbf{k}||\mathbf{q}|$. We use the convention of Bjorken and Drell to define the γ matrices; the Dirac spinors are normalized as $\bar{u}(p)\gamma_\alpha u(p) = 2p_\alpha$.

The scattering amplitude is written as

$$T_{fi} = \frac{I_{fi}}{(2\pi)^6 \sqrt{2E_\omega(\mathbf{q})\, 2|\mathbf{k}| 2E_N(\mathbf{p}) 2E_N(\mathbf{p}')}}, \tag{2}$$

where $E_i(\mathbf{p}) = \sqrt{M_i^2+\mathbf{p}^2}$, with M_i denoting the mass of the particle i. In the center of mass (c.m.) system, the quantization axis $\mathbf{z}$ is chosen along the beam momentum, and the $\mathbf{y}$ axis is perpendicular to the production plane: $\mathbf{y} = \mathbf{p}\times\mathbf{p}'/|\mathbf{p}\times\mathbf{p}'|$. The differential cross section is related to the invariant amplitude by

$$\frac{d\sigma_{fi}}{dt} = \frac{1}{64\pi(W^2-M_N^2)^2} \sum_{m_i m_f \lambda_\gamma \lambda_V} |I_{fi}|^2, \tag{3}$$

where m_i, m_f are the proton spin projections in the initial and final state, respectively, and $\lambda_\gamma \lambda_V$ are the helicities of the incoming photon and outgoing vector meson, respectively. In this paper we will also investigate some of the single- and double-spin observables [35].

The considered beam asymmetry Σ_x for the linearly polarized photons reads

$$\Sigma_x = \frac{d\sigma_{\mathbf{y}} - d\sigma_{\mathbf{x}}}{d\sigma_{\mathbf{y}} + d\sigma_{\mathbf{x}}} = \frac{\mathrm{Tr}[I_{fi}\sigma_\gamma^x I_{fi}^\dagger]}{\mathrm{Tr}[I_{fi} I_{fi}^\dagger]}, \tag{4}$$

where the subscript $\mathbf{y}$ ($\mathbf{x}$) corresponds to a photon linearly polarized along the $\mathbf{y}$ ($\mathbf{x}$) axis. In the case of a circularly polarized photon beam, the double beam-target (recoil) asymmetry is very sensitive to the production mechanism [37]. Therefore, in the present work we analyze the beam-target asymmetry,

$$C_{zz}^{BT} = \frac{d\sigma(\rightrightarrows) - d\sigma(\rightleftarrows)}{d\sigma(\rightrightarrows) + d\sigma(\rightleftarrows)}, \tag{5}$$

where the arrows represent the spin projections of the incoming photon and the target protons: ($\rightrightarrows$) and ($\rightleftarrows$) thus correspond to the initial states with the total spin equal to $\frac{3}{2}$ and $\frac{1}{2}$, respectively.

The double polarization observables related to the beam polarization and polarization of the outgoing vector mesons are described in terms of spin-density matrices ρ_{ij}, which determine the vector-meson decay distributions in its rest frame [39] and are defined by

$$\rho^0_{\lambda\lambda'} = \frac{1}{N} \sum_{\alpha,\lambda_\gamma} I_{\alpha;\lambda,\lambda_\gamma} I^\dagger_{\alpha;\lambda',\lambda_\gamma},$$

$$\rho^1_{\lambda\lambda'} = \frac{1}{N} \sum_{\alpha,\lambda_\gamma} I_{\alpha;\lambda,-\lambda_\gamma} I^\dagger_{\alpha;\lambda',\lambda_\gamma},$$

$$\rho^2_{\lambda\lambda'} = \frac{i}{N} \sum_{\alpha,\lambda_\gamma} \lambda_\gamma I_{\alpha;\lambda,-\lambda_\gamma} I^\dagger_{\alpha;\lambda',\lambda_\gamma},$$

$$\rho^3_{\lambda\lambda'} = \frac{1}{N} \sum_{\alpha,\lambda_\gamma} \lambda_\gamma I_{\alpha;\lambda,\lambda_\gamma} I^\dagger_{\alpha;\lambda',\lambda_\gamma}, \tag{6}$$

where the symbol α includes the polarizations of the incoming and the outgoing baryons, and the normalization factor reads

$$N = \sum_{\alpha,\lambda,\lambda_\gamma} I_{\alpha;\lambda,\lambda_\gamma} I^\dagger_{\alpha;\lambda,\lambda_\gamma}. \tag{7}$$

The $\phi \to K^+K^-$ decay distribution as a function of the polar (Θ) and azimuthal (Φ) angles is expressed through the spin-density-matrix elements and depends on the beam polarization. The polarization vectors of the linear ($\boldsymbol{\varepsilon}$) and circular ($\boldsymbol{\varepsilon}^\lambda, \lambda = \pm 1$) photon polarizations read

$$\boldsymbol{\varepsilon} = (\cos\Psi, \sin\Psi, 0),$$

$$\boldsymbol{\varepsilon}^\lambda = -\frac{\lambda}{\sqrt{2}}(1, i\lambda, 0). \tag{8}$$

For easy reference we list here the explicit form of the decay angular distribution $W(\cos\Theta,\Phi,\Psi)$ for various photon polarizations in the rest frame of the outgoing ϕ meson. For unpolarized photons, it reads

$$W_{\rm unpol}(\cos\Theta,\Phi)=W^0(\cos\Theta,\Phi), \tag{9}$$

with

$$W^0(\cos\Theta,\Phi)=\frac{3}{4\pi}\left\{\frac{1}{2}(1-\rho^0_{00})+\frac{1}{2}(3\rho^0_{00}-1)\cos^2\Theta - \sqrt{2}\,{\rm Re}\rho^0_{10}\sin 2\Theta\cos\Phi - \rho^0_{1\text{-}1}\sin^2\Theta\cos 2\Phi\right\}. \tag{10}$$

For the circularly polarized photons of helicity $\lambda_\gamma=\pm 1$, the angular distribution has the following form:

$$W^{\pm}(\cos\Theta,\Phi)=W^0(\cos\Theta,\Phi) \pm\frac{3}{4\pi}P_\gamma\{\sqrt{2}\,{\rm Im}\rho^3_{10}\sin 2\Theta\sin\Phi + {\rm Im}\rho^3_{1\text{-}1}\sin^2\Theta\sin 2\Phi\}, \tag{11}$$

where P_γ is the strength of polarization $(0\leqslant P_\gamma\leqslant 1)$.

In the case of the linearly polarized photons the decay distribution is defined as

$$W^L(\cos\Theta,\Phi,\Psi)=W^0(\cos\Theta,\phi) - P_\gamma[W^1(\cos\Theta,\Phi)\cos 2\Psi + W^2(\cos\Theta,\Phi)\sin 2\Psi], \tag{12}$$

where Ψ denotes the angle between the photon-polarization vector and ϕ-meson production plane [cf. Eq. (8)]. The partial distributions $W^{1,2}$ read

$$W^1(\cos\Theta,\Phi)=\frac{3}{4\pi}\{\rho^1_{11}\sin^2\Theta+\rho^1_{00}\cos^2\Theta - \sqrt{2}{\rm Re}\,\rho^1_{10}\sin 2\Theta\cos\Phi - \rho^1_{1\text{-}1}\sin^2\Theta\cos 2\Phi\},$$

$$\mathcal{W}^2(\cos\Theta,\Phi)=\frac{3}{4\pi}\{\sqrt{2}{\rm Im}\,\rho^2_{10}\sin 2\Theta\sin\Phi + {\rm Im}\,\rho^2_{1\text{-}1}\sin^2\Theta\sin 2\Phi\}. \tag{13}$$

The spin-density matrix elements depend on the choice of the quantization axis $\mathbf{z}'$ that defines the reference frame of the vector-meson-decay distribution. There are several choices of the quantization axis $\mathbf{z}'$ in the vector-meson rest frame: the helicity system with $\mathbf{z}'$ opposite to the velocity of the recoiling nucleon, the Gottfried-Jackson system (GJ) with $\mathbf{z}'$ parallel to the momentum of the photon, and the Adair system with $\mathbf{z}'$ parallel to the photon momentum in the c.m. Although the general formalism for the analysis of the vector-meson decay does not depend on the system, all our calculations are done in the GJ system, where some of the amplitudes have a simple helicity-conserving form regardless of the momentum transfers.

Using the two-dimensional decay distribution of Eq. (10), one can get the one-dimensional distributions after integrating over the remaining variables,

$$W^0(\cos\Theta)=\frac{3}{2}\left(\frac{1}{2}(1-\rho^0_{00})\sin^2\Theta+\rho^0_{00}\cos^2\Theta\right),$$

$$W^0(\Phi)=\frac{1}{2\pi}(1-2{\rm Re}\rho^0_{1\text{-}1}\cos 2\Phi). \tag{14}$$

In the case of the linearly polarized beam, the distributions depend additionally on the direction of the polarization vector,

$$W^L(\cos\Theta,\Psi)=W^0(\cos\Theta)-\frac{3}{2}(\rho^1_{11}\sin^2\Theta + \rho^1_{00}\cos^2\Theta)P_\gamma\cos(2\Psi),$$

$$W^L(\Phi,\Psi)=W^0(\Phi)+\frac{1}{\pi}P_\gamma(\overline{\rho^1_{1\text{-}1}}\cos[2(\Phi-\Psi)] + \Delta_{1\text{-}1}\cos[2(\Phi+\Psi)]), \tag{15}$$

where

$$\overline{\rho^1_{1\text{-}1}}=\frac{1}{2}(\rho^1_{1\text{-}1}-{\rm Im}\,\rho^2_{1\text{-}1}),\quad \Delta_{1\text{-}1}=\frac{1}{2}(\rho^1_{1\text{-}1}+{\rm Im}\rho^2_{1\text{-}1}). \tag{16}$$

The averaging over the angle between polarization and production planes, at fixed Φ-Ψ results in the following one-dimensional distributions:

$$W^L(\cos\Theta)=W^0(\cos\Theta),$$

$$W^L(\Phi-\Psi)=\frac{1}{2\pi}(1+2P_\gamma\overline{\rho^1_{1\text{-}1}}\cos[2(\Phi-\Psi)]). \tag{17}$$

The integration over Θ and Φ gives dependence of the total decay distribution as a function on Ψ,

$$W^L(\Psi)=1-P_\gamma(2\rho^1_{11}+\rho^1_{00})\cos 2\Psi. \tag{18}$$

For the circularly polarized beam, the distributions read

$$W^{\pm}(\cos\Theta)=W^0(\cos\Theta),$$

$$W^{\pm}(\Phi)=W^0(\Phi)\pm\frac{1}{\pi}P_\gamma\,{\rm Im}\,\rho^3_{1\text{-}1}\sin 2\Phi. \tag{19}$$

We will also discuss the vector-meson decay asymmetry that is related to the matrix elements $\rho^{0,1}_{11},\rho^{0,1}_{1\text{-}1}$,

$$\Sigma_V=\frac{\rho^1_{11}+\rho^1_{1\text{-}1}}{\rho^0_{11}+\rho^0_{1\text{-}1}}, \tag{20}$$

and has a meaning of the asymmetry between the two angular distributions when the decay angles are fixed and equal $\Theta=\pi/2$ and $\Phi=\pi/2$, and $\Psi=\pi/2,0$,

$$\Sigma_V=\frac{1}{P_\gamma}\frac{W^L\left(\cos\Theta,\Phi,\Psi=\frac{\pi}{2}\right)-W^L(\cos\Theta,\Phi,\Psi=0)}{W^L\left(\cos\Theta,\Phi,\Psi=\frac{\pi}{2}\right)+W^L(\cos\Theta,\Phi,\Psi=0)}. \tag{21}$$

III. THE AMPLITUDE

A. Diffractive photoproduction

The invariant amplitude in the region of small momentum transfers ($I^{\rm Diff}$) can be considered in frame of Regge phenomenology as a sum of the Pomeron and other Regge trajectories. For $E_\gamma\simeq 2$–3 GeV ($s\simeq 5$–7 GeV^2), this region is limited by the forward angle photoproduction with $|t|\lesssim 0.5$–0.7 GeV^2, where $|t|/s\lesssim 0.1\ll 1$ [40]. As we will see later, the employment of conventional residuals in corresponding amplitudes expressed through the isoscalar nucleon form factors leads to fast decreasing of $I^{\rm Diff}$, so that it becomes rather small in the region beyond its validity. On the other hand, the meson photoproduction at low energy and large momentum transfers with $|t|\sim|t|_{\rm max}$ ($\theta\sim\pi$) can be described successfully in terms of the nucleon and resonance-exchange amplitudes $I^{\rm B}$. In diffractive region of the ϕ-meson photoproduction, $I^{\rm B}$ is suppressed by the OZI rule and is negligible compared to $I^{\rm Diff}$. The total amplitude may be written as

$$I_{fi}=I_{fi}^{\rm Diff}\oplus I_{fi}^{\rm B}, \tag{22}$$

where $\oplus$ means that the above two components are defined and operate in different regions of t, and simultaneous account of the Regge amplitude and the resonant part leads, strictly speaking, to double counting [40]. But since in the considered case the interference of $I^{\rm Diff}$ and $I^{\rm B}$ at forward- and backward-angle photoproduction is negligible, we can substitute $\otimes\to+$. This leads to the so-called "interference model" which was widely used in the resonance region (see, for example, Ref. [41]). But taking into account the problem of double counting at the region of $\theta\sim\pi/2$ when interference of the resonant and Regge parts may be sizable, predictions for such a model must be considered as very qualitative estimations, especially for spin variables.

In the diffractive region of the ϕ-meson photoproduction, the two processes are reasonably well established; the Pomeron exchange which is dominant and relatively weak pseudoscalar π,η-meson exchange. For the Pomeron-exchange process, depicted in Fig. 1(a), we use the Donnachie-Landshoff model [1], based on the Pomeron-isoscalar-photon analogy. It gives the amplitude in the following form

$$I_{fi}^P=-M_P(s,t)\Gamma_{fi}^P,$$

$$\Gamma_{fi}^P=\varepsilon_\mu^*(\lambda_V)\bar{u}_f h_P^{\mu\nu}u_i\varepsilon_\nu(\lambda_\gamma), \tag{23}$$

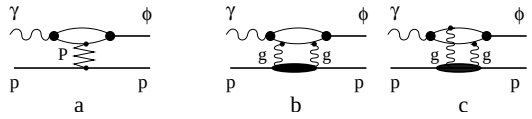

FIG. 1. Diagrammatic representation of (a) Pomeron exchange and (b),(c) two-gluon-exchange contributions in the $\gamma p\to\phi p$ reaction.

where $\varepsilon_\mu(V)$ and $\varepsilon_\nu(\gamma)$ are the polarization vectors of the vector meson (ω,ϕ) and photon, respectively, and $u_i=u_{m_i}(p)$ [$u_f=u_{m_f}(p')$] is the Dirac spinor of the nucleon with momentum p (p') and spin projection m_i (m_f).

The scalar function $M_P(s,t)$ is described by the following Regge parametrization:

$$M_P(s,t)=C_P F_1(t)F_V(t)\frac{1}{s}\left(\frac{s}{s_P}\right)^{\alpha_P(t)}\exp\left[-\frac{i\pi}{2}\alpha_P(t)\right], \tag{24}$$

where $F_1(t)$ is the isoscalar electromagnetic form factor of the nucleon and $F_V(t)$ is the form factor for the vector-meson–photon–Pomeron coupling. We also follow Ref. [1] to write

$$F_1(t)=\frac{4M_N^2-2.8t}{(4M_N^2-t)(1-t/t_0)^2},$$

$$F_V(t)=\frac{2\mu_0^2}{(1-t/M_V^2)(2\mu_0^2+M_V^2-t)}, \tag{25}$$

where $t_0=0.7$ GeV^2. The Pomeron trajectory is known to be $\alpha_P(t)=1.08+0.25t$. (Also see Ref. [7].) The strength factor C_P equals

$$C_P=\frac{6g^2\sqrt{4\pi\alpha_{\rm em}}}{\gamma_V}, \tag{26}$$

where γ_V is the vector-meson decay constant ($2\gamma_\omega=17.05$ and $2\gamma_\phi=13.13$) and $\alpha_{\rm em}=e^2/4\pi$. The parameter g^2 is the product of two dimensionless coupling constants $g^2\equiv g_{Pss}g_{Pqq}=(\sqrt{s_P}\beta_s)(\sqrt{s_P}\beta_u)$, where g_{Pss} and g_{Pqq} have a meaning of the Pomeron coupling with the strange quarks in a ϕ meson and the light in a proton, respectively. For the ω-meson photoproduction, $g^2\equiv q_{Pqq}^2$.

The vertex function $h_P^{\mu\nu}$ is defined by a trace calculation of the quark loop in the diagram of Fig. 1(a) with the nonrelativistic vector-meson wave function and the vector coupling for the Pomeron-quark-quark vertex ($V_{Pqq}\sim\gamma_\alpha$). The net result reads

$$h_P^{\mu\nu}=\not{k}\left(g^{\mu\nu}-\frac{q^\mu q^\nu}{q^2}\right)-\gamma^\nu\left(k^\mu-\frac{q^\mu k\cdot q}{q^2}\right)-q^\nu\left(\gamma^\mu-\frac{\not{q}q^\mu}{q^2}\right), \tag{27}$$

where we keep the explicit gauge-invariant terms and skip the term proportional to k^ν, which, after being multiplied by the photon-polarization vector does not contribute. One can

see that the last term violates gauge invariance. That is a serious problem and its solution requires a more detailed description of the gluon-exchange mechanism and vertex functions [5,6,42], which is beyond the scope of this work. Here, we perform gauge-invariance restoration by gauge transformation, since the above described simple model has been very successful in the description of many processes. The easiest way is the transformation of q^ν in the last term of Eq. (27),

$$q^\nu \to \bar{q}^\nu = q^\nu - \bar{p}^\nu \frac{k\cdot q}{\bar{p}\cdot k}, \tag{28}$$

where the vector $\bar{p}$ must be fixed via an additional assumption. Using this transformation, the vertex function Γ^P_{fi} has the following form:

$$\Gamma^P_{fi} = \bar{u}_f \not{k} u_i (\varepsilon^*_{\lambda_V}\cdot\varepsilon_{\lambda_\gamma}) - \bar{u}_f \not{\varepsilon}_{\lambda_\gamma} u_i (\varepsilon^*_{\lambda_V}\cdot k) - \bar{u}_f \not{\varepsilon}^*_{\lambda_V} u_i \left(\varepsilon_{\lambda_\gamma}\cdot q - \frac{(\varepsilon_{\lambda_\gamma}\cdot\bar{p})(k\cdot q)}{\bar{p}\cdot k}\right). \tag{29}$$

To find the vector $\bar{p}$, we take into account that it must lie in the production plane and should be constructed from the three linear independent vectors p, p', and q, be different from q and, it must have a proper ''high energy limit.'' This limit may be found using the Pomeron–two-gluon-exchange analogy [43], since it is now generally believed that the Pomeron exchange is generated by the gluon exchange [44,45] and the nonperturbative two-gluon-exchange process [2] justifies the vector type of coupling in Pqq-vertex.

The two-gluon-exchange amplitude for the vector-meson photoproduction is depicted in Figs. 1(b),(c). The amplitude, where the two gluons interact with the same quark [Fig. 1(b)], generates the vertex $h^{\mu\nu}_{2g}$ with the same structure as the Pomeron-exchange mechanism. The amplitude where the two gluons interact with different quarks [Fig.1(c)] contains an additional term proportional to $\bar{u}(p')\not{\varepsilon}_{\lambda_\gamma} u(p_1)\cdot\bar{u}(p_1)\not{\varepsilon}^*_{\lambda_V} u(p)$, where p_1 is the momentum of the quark in the intermediate state. This term restores the gauge invariance. At high energies and small momentum transfers where $p'\simeq p_1\simeq p$ and $\bar{u}(p')\gamma_\alpha u(p)\simeq 2p_\alpha$, the two-gluon-exchange model results [46,42],

$$\Gamma^{2g}_{fi} \sim (k\cdot p)(\varepsilon^*_{\lambda_V}\cdot\varepsilon_{\lambda_\gamma}) - (\varepsilon_{\lambda_\gamma}\cdot p)(\varepsilon^*_{\lambda_V}\cdot k) - (\varepsilon^*_{\lambda_V}\cdot p)\left(\varepsilon_{\lambda_\gamma}\cdot q - \frac{(\varepsilon_{\lambda_\gamma}\cdot p)(k\cdot q)}{p\cdot k}\right). \tag{30}$$

One can see the identity of Eqs. (29) and (30) if $\bar{p}=p$ (cf. Ref. [21]). But at relatively low energies where $p'\neq p$, a more reasonable choice is $\bar{p}=\frac{1}{2}(p+p')$, symmetrical with respect to p and p', because of approximate estimates $\bar{u}(p')\gamma_\alpha u(p)\simeq (p+p')_\alpha$. This value of $\bar{p}$, together with Eq. (29), will be used in our calculations. Note that at large photon energies, the last two terms in Eq. (29) are negligible, but at a few GeV and finite $|t|$, they generate spin-flip transitions and become important.

By fitting all available total cross section data for ω, ρ, and ϕ photoproduction at high energies, the remaining parameters of the model are determined: $\mu_0^2=1.1$ GeV^2, $s_P=4$ GeV^2, $\beta_s=1.61$, and $\beta_u=2.05$ GeV^{-1}, which give $g_{Pqq}=4.1$ and $g_{Pss}=3.22$.

The pseudoscalar-meson-exchange amplitude may be expressed either in terms of the one-boson-exchange model [10,20,22,37] or using the Regge model [21,24]. The pseudoscalar-meson exchange amplitude in the one-boson-exchange (OBE) approximation is evaluated from the following effective Lagrangians:

$$\mathcal{L}_{V\gamma\varphi} = \frac{e g_{V\gamma\varphi}}{M_V}\epsilon^{\mu\nu\alpha\beta}\partial_\mu V_\nu \partial_\alpha A_\beta \varphi,$$

$$\mathcal{L}_{\varphi NN} = -ig_{\pi NN}\bar{N}\gamma_5\tau_3 N\pi^0 - ig_{\eta NN}\bar{N}\gamma_5 N\eta, \tag{31}$$

where $\varphi=(\pi^0,\eta)$ and A_β is the photon field. The resulting invariant amplitude is

$$I^{ps}_{fi} = -\sum_{\varphi=\pi,\eta}\frac{iF_{\varphi NN}(t)F_{V\gamma\varphi}(t)}{t-M_\varphi^2}\frac{e g_{V\gamma\varphi} g_{\varphi NN}}{M_V}\bar{u}_{m_f}(p') \times\gamma_5 u_{m_i}(p)\varepsilon^{\mu\nu\alpha\beta}q_\mu k_\alpha \varepsilon^*_\nu(V)\varepsilon_\beta(\gamma). \tag{32}$$

In the above, we have followed Ref. [47] to include the following form factors to dress the φNN and $V\gamma\varphi$ vertices:

$$F_{\varphi NN}(t) = \frac{\Lambda_\varphi^2 - M_\varphi^2}{\Lambda_\varphi^2 - t}, \quad F_{V\gamma\varphi}(t) = \frac{\Lambda_{V\gamma\varphi}^2 - M_\varphi^2}{\Lambda_{V\gamma\varphi}^2 - t}. \tag{33}$$

We use $g_{\pi NN}=13.26$ and $g_{\pi NN}=3.527$ for the πNN and ηNN coupling constants, respectively (cf. Ref. [20] for discussion and references). The coupling constants $g_{V\gamma\varphi}$ can be estimated through the decay widths of $V\to\gamma\pi$ and $V\to\gamma\eta$ [38], which lead to $g_{\omega\gamma\pi}=1.823$, $g_{\phi\gamma\pi}=-0.141$, $g_{\omega\gamma\eta}=0.416$, and $g_{\phi\gamma\eta}=-0.707$. The cutoff parameters Λ_φ and $\Lambda_{\omega\gamma\varphi}$ in Eq. (33) are chosen to reproduce the ω-meson photoproduction at low energies [16]: $\Lambda_\pi=0.6$ GeV^2, $\Lambda_\eta=0.9$ GeV^2, $\Lambda_{V\gamma\pi}=0.6$ GeV^2, and $\Lambda_{V\gamma\eta}=1.0$ GeV^2.

In Refs. [21,24,48] it is suggested to describe pseudoscalar-meson (PS) exchange with a π-meson-exchange trajectory by making use of Reggezation of the Feynman propagator in the following way:

$$\frac{1}{t-m_\pi^2} \Rightarrow \left(\frac{s}{s_1}\right)^{\alpha_\pi(t)} \frac{(1+e^{-i\pi\alpha_{\pi(t)}})\pi\alpha'_\pi}{2\sin(\pi\alpha_\pi)\Gamma[\alpha_\pi(t)+1]}, \tag{34}$$

where the trajectory is given by

$$\alpha_\pi(t) = \alpha'_\pi(t-m_\pi^2), \tag{35}$$

with $\alpha'_\pi=0.7$ GeV^{-2}. Using properties of the Γ function: $\Gamma(1+z)=z\Gamma(z)$ and $\Gamma(z)\Gamma(1-z)\sin\pi z=\pi$, and assuming

that $|\alpha_\pi(t_{\max})| \ll 1$, one can see that the Reggezation of Eq. (34) does not modify the pole t-dependence of the OBE amplitude at forward-angle photoproduction. The Regge phenomenology does not define t dependence and phases of residuals. In practice, they are determined by comparison of the Regge and OBE amplitudes at low energies where the lowest t-channel resonances are expected to be dominant [49,48]. In the present paper we analyze photoproduction in narrow energy region for $W=2-3$ GeV, and in order to avoid consideration of additional parameters we will directly use the OBE model for the pseudoscalar-meson-exchange processes, with the parameters taken from independent studies. In this case our result coincides with the Regge model at small $|t|$, and slightly overestimates it at backward-angle photoproduction where the contribution of pseudoscalar-meson-exchange becomes negligible relative to the other channels.

Together with these conventional processes, several other diffractive channels are discussed in the literature. One of them is OZI-rule allowed f_2'-meson exchange or contribution of the f_2'-meson Regge trajectory [21]. Significant strangeness content of $f_2'(1525)$ supports the existence of this channel. But, on the other hand, the absence of a finite $f_2' \to \gamma\phi$ decay width [38] is a real problem for applying a f_2' trajectory in ϕ-meson photoproduction and the only argument for its use is to obtain agreement with the low-energy data.

Another possible low-energy channel is related to the pure gluon dynamics such as a glueball exchange or the contribution of a glueball ($J^\pi = 0^+, M_{\rm gl}^2 \simeq 3$ GeV^2) inspired trajectory [23]. The idea is based on the assumption that the Pomeron trajectory is also inspired by the glueball exchange, being the leading glueball Regge trajectory. Other trajectories may appear as its daughter trajectories. This picture has been justified recently by calculations within the string model [8,50]. The slope of the glueball trajectory is found to be much smaller than slope of conventional mesonic trajectories and close to the Pomeron trajectory.

Since both f_2' and glueball trajectories are not forbidden, we also include them into the total amplitude. To fix the vertex $h^{\mu\nu}$ we use the simplest covariant and gauge-invariant effective Lagrangians for $VV\xi$ interactions, where V and ξ are the vector and boson ($0^+, 2^+$) fields, respectively,

$$\mathcal{L}_{0^+} = \frac{1}{4} g_{\alpha\beta} (\Lambda^{\alpha\beta} + \Lambda^{\beta\alpha}) \xi, \tag{36a}$$

$$\mathcal{L}_{2^+} = \frac{1}{4} (\Lambda^{\alpha\beta} + \Lambda^{\beta\alpha}) \xi_{\alpha\beta} + (\Lambda^{\alpha\beta} - \Lambda^{\beta\alpha}) \xi_{\alpha\beta}, \tag{36b}$$

with

$$\Lambda^{\alpha\beta} = \partial_\mu V_1^\alpha \partial^\mu V_2^\beta + \partial^\alpha V_1^\mu \partial^\beta V_{2\mu} - \partial^\alpha V_1^\mu \partial_\mu V_2^\beta - \partial_\mu V_1^\alpha \partial^\beta V_2^\mu. \tag{37}$$

Taking the corresponding fermion-boson interactions as $\bar{\psi}\psi\xi$ and $\bar{\psi}\gamma^\alpha\gamma^\beta\psi\xi_{\alpha\beta}$, we get the vertices $h^{\mu\nu}$ as follows:

$$h_{0^+}^{\mu\nu} = g^{\mu\nu} k\cdot q - k^\mu q^\nu, \tag{38a}$$

$$h_{2^+}^{\mu\nu} = h_{0^+}^{\mu\nu} - 2i\sigma_{\alpha\beta} [g^{\alpha\mu} g^{\beta\nu} k\cdot q + q^\alpha k^\beta g^{\mu\nu} + g^{\alpha\nu} q^\beta k^\mu + g^{\beta\mu} k^\alpha q^\nu]. \tag{38b}$$

Note that the similar expressions can be also found using the loop integration within the same prescription as for the Pomeron exchange in the Donnachie-Landshoff model with the Reggeon-quark-quark vertices taken as 1, and $\gamma_\alpha\gamma_\beta$ for 0^+ and 2^+ exchanges, respectively. The difference is in additional gauge breaking term which appears in Eq. (38b), $g^{\alpha\mu} q^\beta q^\nu$. It brings some ambiguity for this method, but for us it is important that the structure of all other terms, including their mutual signs, is identical to Eq. (38b).

The scalar $[M(s,t)]$ functions read

$$M_R(s,t) = C_R F_1(t) F_V(t) \frac{1}{N_R} \left(\frac{s}{s_R}\right)^{\alpha_R(t)} \times \frac{\eta_R (1 + e^{-i\pi\alpha_{R(t)}}) \pi\alpha_R'}{2\sin(\pi\alpha_R)\Gamma[\alpha_R(t)]}, \tag{39}$$

where $R = f_2'$, gl, and C_R differ from C_P in Eq. (24) by the substitution $g_P^2 \to g_R^2$. The normalization factors N_R in Eq. (23) are defined by h_R: $N_{2^+} \simeq 2sM_V$, $N_{0^+} \simeq M_N M_V^2$. Following Ref. [21] we choose f_2' trajectory as $\alpha_{f_2'} = 0.55 + \alpha_{f_2'}' t$, with $\alpha_{f_2'} = 0.7$ GeV^{-2}, and the mass scale $s_{f_2'} = 1$ GeV^2. For the glueball trajectory we will use the parameters of Ref. [23], with $\alpha_{\rm gl}(0) = -0.75$, $\alpha_{\rm gl}' = 0.25$ GeV-2, and $s_{gl} = \alpha_{\rm gl}'^{-1}$. The phase $\eta_R = \pm 1$ and the strength g_R are not defined in the Regge model and have to be found to bring the model calculation close to the data for unpolarized total cross section.

Finally, we note that sometimes in literature the Regge amplitude at low energy is chosen with an additional threshold factor to get a better shape of the energy dependence in the near-threshold region, which modifies the standard parametrization as follows:

$$\left(\frac{s}{s_R}\right)^{\alpha(t)} \to \left(\frac{s - a_R}{s_R}\right)^{\alpha(t)}. \tag{40}$$

It is obvious that the relative contribution of each trajectory in the threshold region strongly depends on the threshold parameter a_R, which is not defined by the Regge model. Thus, the finite value of a_P in Pomeron exchange leads to a decrease of the contribution of the Pomeron-exchange amplitude, which must be compensated by the increase of strength in additional trajectories [20,22,23]. The shape of the energy dependence of the total cross section is sensitive to the choice of a_P, a_R at energies close to the threshold. In the present paper we choose the value $a_R = 0$ for all trajectories. This choice corresponds to the upper limit for the contribution of Pomeron exchange and the lower limit for the additional Regge trajectories in near-threshold region. Its validity must be checked in study of the polarization observables in diffractive region, because the vertex functions for the Pomeron and other trajectories in Eqs. (29), (38a), and (38b) lead to quite different predictions. In the Appendix, we illus-

trate this point for two other extreme cases where the diffractive amplitude is dominated by the f_2' and 0^+ (glueball) trajectories, respectively. They can be realized at large a_P, $a_P \sim s_P$.

B. Baryon and baryon-resonance exchange

The amplitude I^{B} in Eq. (22) consists of baryon (I^N) and baryon-resonance-exchange (I^{N^*}) terms,

$$I^{\mathrm{B}} = I^N + I^{N^*}. \tag{41}$$

To evaluate these channels we use the effective Lagrangian approach, developed for ω-meson photoproduction and discussed in our recent paper [16]. Here, we restrict the consideration to a brief description, given below. We consider all isospin $I=1/2$ nucleon resonances listed by the Particle Data Group [38] with empirically known helicity amplitudes of $\gamma N \to N^*$ transitions. We thus have contributions from 12 resonances: $P_{11}(1440)$, $D_{13}(1520)$, $S_{11}(1535)$, $S_{11}(1650)$, $D_{15}(1675)$, $F_{15}(1680)$, $D_{13}(1700)$, $P_{11}(1710)$, $P_{13}(1720)$, $F_{17}(1990)$, $D_{13}(2080)$, and $G_{17}(2190)$.

In Ref. [16] we found that the contribution of the nucleon term with standard parametrization [51,52] is much smaller than a resonant part. Therefore, in the present paper we only consider the resonance-exchange contribution.

For the N^* with spin J and parity P, $J^P = \frac{1}{2}^{\pm}$, $\frac{3}{2}^{\pm}$, $\frac{5}{2}^{\pm}$, $\frac{7}{2}^{\pm}$, we use the following effective Lagrangians:

$$\mathcal{L}^{1/2^{\pm}}_{\gamma NN^*} = \frac{e g_{\gamma NN^*}}{2M_{N^*}} \bar{\psi}_{N^*} \Gamma^{(\pm)} \sigma_{\mu\nu} F^{\mu\nu} \psi_N + \mathrm{H.c.}, \tag{42}$$

$$\mathcal{L}^{3/2^{\pm}}_{\gamma NN^*} = i \frac{e g_{\gamma NN^*}}{M_{N^*}} \bar{\psi}^{\mu}_{N^*} \gamma_\lambda \Gamma^{(\mp)} F^{\lambda\mu} \psi_N + \mathrm{H.c.}, \tag{43}$$

$$\mathcal{L}^{5/2^{\pm}}_{\gamma NN^*} = \frac{e g_{\gamma NN^*}}{M^2_{N^*}} \bar{\psi}^{\mu\alpha}_{N^*} \gamma_\lambda \Gamma^{(\pm)} (\partial_\alpha F^{\lambda\mu}) \psi_N + \mathrm{H.c.}, \tag{44}$$

$$\mathcal{L}^{7/2^{\pm}}_{\gamma NN^*} = -i \frac{e g_{\gamma NN^*}}{M^3_{N^*}} \bar{\psi}^{\mu\alpha\beta}_{N^*} \gamma_\lambda \Gamma^{(\mp)} (\partial_\beta \partial_\alpha F^{\lambda\mu}) \psi_N + \mathrm{H.c.}, \tag{45}$$

where ψ_N are the nucleon fields; ψ_{N^*}, ψ_α, $\psi_{\alpha\beta}$, and $\psi_{\alpha\beta\gamma}$ are the Rarita-Schwinger spin $\frac{1}{2}$, $\frac{3}{2}$, $\frac{5}{2}$, and $\frac{7}{2}$ field, respectively, and M_{N^*} is the resonance mass. A_μ is the photon field and $F^{\mu\nu} = \partial^\nu A^\mu - \partial^\mu A^\nu$. The coupling $\Gamma^+ = 1 (\Gamma^- = \gamma_5)$ defines the N^* excitations with different parity.

We define the ωNN^* interactions by using the vector-dominance model. This assumes that the effective $\mathcal{L}_{\omega NN^*}$ Lagrangian has the same form as the corresponding $\mathcal{L}_{\gamma NN^*}$ with substitutions $A_\mu \to \omega_\mu$ and $e g_{s\gamma NN^*} \to f_\omega$, where $f_\omega = 2 g_s \gamma_\omega$. The isoscalar-coupling constant g_s is related to the strengths of the N^* excitations on the proton ($g_p = g_{\gamma pN^*}$) and on the neutron ($g_n = g_{\gamma nN^*}$), and equals $g_s = (g_p + g_n)/2$.

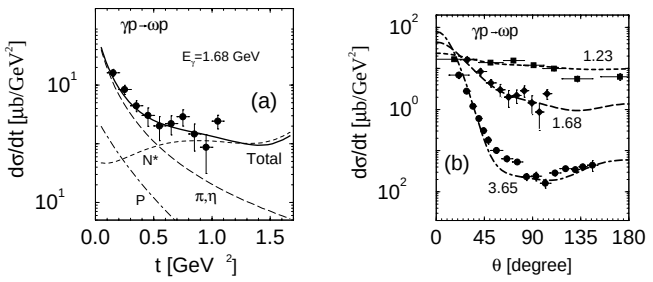

FIG. 2. (a) The differential cross section of $\gamma p \to \omega p$ reaction as a function of $-t$ at $E_\gamma = 1.68$ GeV. The lines denote the pseudoscalar-meson exchange (long dashed), Pomeron exchange (dot-dashed), resonant channel (dashed), and the full amplitude (solid), respectively. (b) The differential cross sections as a function of the ω-meson production angle at $E_\gamma = 1.23$, 1.68 GeV, and 3.65 GeV. Data are taken from Refs. [53,54].

The γNN^* and ωNN^* vertices are regularized by the form factor $F_{N^*}(r^2) = \Lambda^4/[\Lambda^4 + (r^2 - M^2_{N^*})^2]$, where r is the four-momentum of the intermediate baryon state, the cutoff parameter $\Lambda = 0.85$ GeV is chosen to be the same for all resonances. More detailed discussion of the effective Lagrangians, propagators, fixing the γNN^* couplings, and comparison with other approaches are given in Ref. [16].

Validity of the model is illustrated in Fig. 2, where we show result of our calculation for the differential cross section of $\gamma p \to \omega p$ reaction together with experimental data at $E_\gamma = 1.23$, 1.68 GeV [53], and 3.65 GeV [54]. In Fig. 2(a) we show the differential cross section as a function of t at $E_\gamma = 1.68$ GeV (solid curve) together with the partial contribution of each of the main channels: pseudoscalar-meson exchange, Pomeron exchange, and resonance excitation, depicted by long-dashed, dot-dashed, and dashed curves, respectively. In Fig. 2(b) we show the differential cross section as a function of the ω production angle in the c.m. system at $E_\gamma = 1.23$, 1.68, and 3.65 GeV by the dashed, dot-dashed, and solid lines, respectively. The contribution of the resonance excitations is important at backward angles, and it results in the agreement of data with our calculation at large momentum transfers. We also found that at $E_\gamma = 3.65$ GeV, only the Pomeron-exchange contribution is not sufficient to get agreement at forward angle photoproduction with $|t| < 1$ GeV^2. Therefore, following Ref. [21], we include also a f_2-meson trajectory. It is calculated similar to that of the f_2'-meson trajectory [Eqs. (39)] with $g^2_{f_2} \simeq 3 g^2_P$ and $\eta_{f_2} = +1$. One can see that the model satisfactorily reproduces both the energy and the angular distribution of the ω photoproduction in the considered energy region. However, it leaves some scope for additional processes, such as two-step photoproduction mechanisms [55] and direct-quark exchange, which are expected to be important at large energy and at $\theta \sim \pi/2$ [54], and must be subject for special detailed analysis. There, it is most important that the model reproduces the cross section at backward-angle photoproduction, which allows us to fix the resonant part of the ϕ-meson photoproduction.

For the ϕ-meson photoproduction we assume the same N^*-excitation mechanism with the substitution $f_{\omega NN^*}$

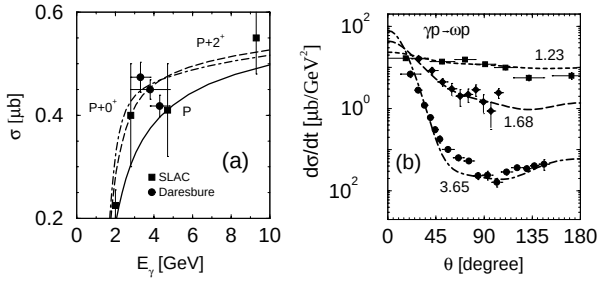

FIG. 3. (a) The total cross section of $\gamma p \to \phi p$ reaction as a function of the photon energy E_γ for models I–III indicated by dashed, long-dashed, and dot-dashed curves, respectively. Data are taken from Refs. [57,58]. (b) The total cross section for the hybrid model.

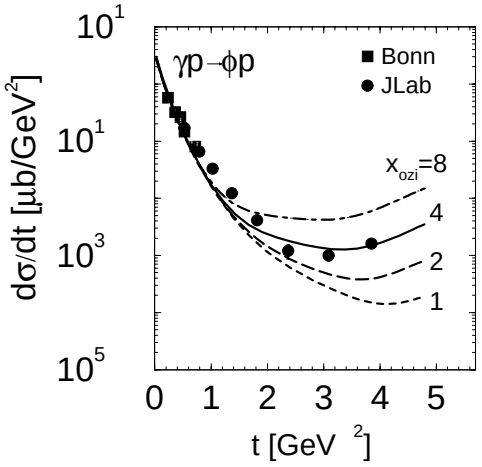

FIG. 4. The differential cross section of $\gamma p \to \phi p$ reaction as a function of t at $E_\gamma = 3.6$ GeV for different values of the OZI-rule evading parameter $x_{\rm OZI}$. Data are taken from Ref. [59].

$\to f_{\phi NN*}$. The key problem is how to fix these coupling constants. For this aim we use the ''minimal'' parametrizations of the $\phi NN*$ coupling constants,

$$f_{\phi NN*} = -\tan\Delta\theta_V x_{\rm OZI} f_{\omega NN*}, \tag{46}$$

where $\Delta\theta_V$ is the deviation of the ϕ-ω mixing angle from the ideal mixing ($\Delta\theta_V \simeq 3.7°$ [38]) and $x_{\rm OZI}$ is the OZI-rule evading parameter [22,56], which will be found from comparison of calculation and data at large momentum transfers. An increase in the value of $x_{\rm OZI}$ from 1 determines the scale of the OZI-rule violation in interaction of the ϕ-meson with baryons.

IV. RESULTS AND DISCUSSIONS

A. Unpolarized cross sections

We first consider the total cross section. Its dominant contribution comes from the diffractive channels at $|t| < 1$ GeV^2. The resonance excitations which are important at large $|t|$ do not affect the total cross section. The total cross section data allow a wide range of OZI-rule evading parameter of the $\phi NN*$ couplings defined in Eq. (44). Therefore, for definiteness sake, we take $x_{\rm OZI} = 4$, which is close to its low bound reported in Refs. [30–32], and as we will see later, this value is in agreement with the available data on ϕ-meson photoproduction at large momentum transfers.

For the analysis of the diffractive mechanism we have to keep in mind that the P and pseudoscalar PS meson exchange are well established. Therefore, any ''exotic'' process is included as a supplementary channel. We will analyze three possibilities: model I includes the P and PS (i.e., without exotic channel); model II includes P and PS meson exchange and f_2' Regge trajectory; model III includes P-PS meson exchange and the glueball inspired trajectory.

All the formulas for models I–III have been described above. The strength parameter g_R and phase factor η_R of f_2' meson and glueball trajectories are fixed by fitting the available data: $g_{f_2'} = 1.87, \eta_{f_2'} = +1$; $g_{gl} = 7.66, \eta_{gl} = -1$.

In Fig. 3(a) we show the total cross section of $\gamma p \to \phi p$ reaction as a function of the photon energy for three models together with the available experimental data [57,58]. Comparison with the data slightly favors for models II and III, but unfortunately, the accuracy of the data is not sufficient to make a definite conclusion about the preference for one of the models. The difference between the models disappears at high energy with $W \gtrsim 10$ GeV ($E_\gamma \gtrsim 50$ GeV), where only the Pomeron trajectory is important. At low energy, high precision data are required to select the favored diffractive mechanism. Taking into account some ambiguity for the reaction mechanism, all our calculations are done using the ''hybrid'' model, where the amplitude is taken as a sum of the Pomeron and PS meson-exchange amplitudes and small contribution of the f_2' and glueball trajectories taken with the equal weights with $g_{f_2'} = 1.32$ and $g_{gl} = 5.42$. The total cross sections calculated from this hybrid model is shown in Fig. 3(b). In the further discussions, for simplicity, we will denote the sum of Pomeron-, f_2'-, and glueball-exchange amplitudes as the ''diffractive'' amplitude. The opposite case where the f_2'- or 0^+-exchange trajectories are dominant is discussed in the Appendix.

In $\gamma p \to \omega p$ reaction at low energies, the backward-angle photoproduction is dominated by the resonant channel (cf. Fig. 2), and we expect a similar picture for $\gamma p \to \phi p$ reaction. The global structure of $N*$-exchange amplitude is fixed by the ω-meson photoproduction and the remaining parameter for the ϕ-meson photoproduction is the OZI-rule evading parameter $x_{\rm OZI}$ in Eq. (46). Figure 4 shows the differential cross section at $E_\gamma = 3.6$ GeV as a function of t for different values of $x_{\rm OZI}$, together with experimental data [59].

The calculation brings agreement with data at $x_{\rm OZI} \simeq 4$. This value is consistent with the results reported in Refs. [30–32] and the estimation of Refs. [26,27]. It would be interesting to check this prediction at lower energies, where the relative contribution of the resonant channels is expected to be stronger.

In Fig. 5(a) we show the differential cross section as function of t at $E_\gamma = 2.0$ GeV together with the partial contribution of main channels with $x_{\rm OZI} = 4$. The diffractive part is described by the hybrid model. One can see that the forward-angle photoproduction is completely defined by the diffrac-

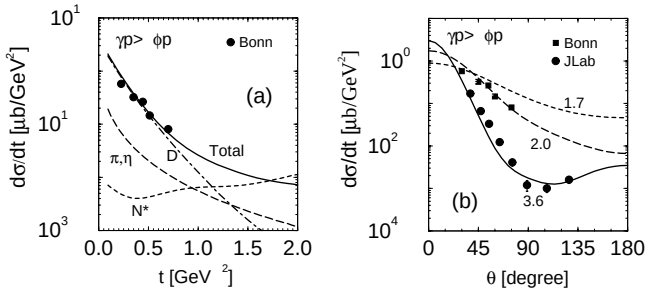

FIG. 5. (a) The differential cross section of $\gamma p \to \phi p$ reaction as a function of $-t$ at $E_\gamma = 2.2$ GeV. The results are the pseudoscalar-meson exchange (long dashed), diffractive channels (dot-dashed), resonance excitation (dashed), and the full amplitude (solid). (b) The differential cross section a function of the ϕ-meson production angle at $E_\gamma = 1.7, 2.0,$ and 3.6 GeV. Data are taken from Refs. [63,59].

tive amplitude; the contribution from the diffractive channels exceeds the pseudoscalar-meson exchange by an order of magnitude. Backward-angle photoproduction is dominated by the N^*-exchange channel, while in the central region ($0.7 \lesssim |t| \lesssim 1.4$ GeV^2), the coherent interference of all processes becomes important. Unfortunately, our model is not very well defined in this region. Figure 5(b) shows the differential cross section as a function of the ϕ-meson production angle in the c.m. system at $E_\gamma = 1.7,$ 2.0, and 3.6 GeV (dashed, long dashed, and dot-dashed lines, respectively). The calculations are in agreement with available data. Since the data at $E_\gamma = 3.6$ GeV are used to fix $x_{\rm OZI}$, the other curves represent our prediction, which would be interesting to check.

B. Spin observables

Spin observables can be used as a powerful tool to test the photoproduction mechanisms in detail. We first consider the spin-density matrix elements $\rho^{0-3}_{\lambda\lambda'}$, which are planned to be measured in near future at the JLab [60] and at the LEPS/SPring-8 [61]. All our calculations have been done in the Gottfried-Jackson system. For simplicity, we show our prediction at all momentum transfers, however, the applicability of the model at $E_\gamma \sim 2$–3 GeV is limited by the forward and backward photoproduction with $|t_{\rm min}| \leqslant |t| \leqslant |t_l|$ and $|t|_{\rm max} - |t_l| \leqslant |t| \leqslant |t|_{\rm max}$, respectively, where $|t_l| \simeq 0.5$–0.7 GeV^2, depending on the energy.

First of all, we remind that the nonzero spin-density matrix elements for the pure helicity conserving amplitude,

$$I_{fi} \sim \delta_{\lambda_i \lambda_f} \delta_{m_i m_f}, \tag{47}$$

have the following values:

$$\rho^0_{11} = \rho^0_{-1-1} = \frac{1}{2}, \quad \rho^1_{1-1} = \rho^1_{-11} = \pm\frac{1}{2},$$

$$\mathrm{Im}\,\rho^2_{-11} = -\,\mathrm{Im}\,\rho^2_{1-1} = \pm\frac{1}{2}, \quad \rho^3_{11} = -\rho^3_{-1-1} = \pm\frac{1}{2}, \tag{48}$$

where the upper and lower signs in ρ^{1-3} correspond to the amplitudes with natural ($I^{\rm N}$) and unnatural ($I^{\rm U}$) parity exchange, respectively. The typical example of the natural and unnatural parity exchange amplitude in our case are the scalar- and the pseudoscalar-meson exchange amplitudes, respectively. For the forward-angle photoproduction, they can be expressed as

$$I^{\rm N}_{m_f m_i;\lambda_\phi \lambda_\gamma}(t) = \begin{pmatrix} 1 \\ 2 m_i \lambda_\gamma \end{pmatrix} \delta_{m_i m_f} \delta_{\lambda_\gamma \lambda_\phi} I^{\rm U}_0(t),$$

where $I^{\rm N}_0(t)$ is the spin-independent part of the corresponding amplitudes.

The Pomeron-exchange amplitude in GJ system has the following structure:

$$I^P_{fi} \sim -\,\delta_{\lambda_\phi \lambda_\gamma} \bar{u}_f \not{k} u_i + \delta_{\lambda_\phi 0} k_\gamma \bar{u}_f \not{\epsilon}_{\lambda_\gamma} u_i + \sqrt{2} \lambda_\gamma p_x \frac{k\cdot q}{2p\cdot k - k\cdot q} \bar{u}_f \not{\epsilon}^*_{\lambda_\phi} u_i, \tag{49}$$

where k_γ and p_x are the photon momentum and the x component of the proton ($p_x = p'_x$ in the GJ system) momentum, respectively. One can see that only the first term satisfies Eq. (47). The second term describes the interaction of the photon and nucleon spins and the interaction of the ϕ-meson spin and the orbital momentum in the initial state. The third term is responsible for the interaction of the ϕ meson and nucleon spins, and for the interaction of the photon spin with the orbital momentum in the final state. At $E_\gamma = 2$–3 GeV, the contribution of these two terms is finite and must be taken into account. Thus, the second and third terms in Eq. (49) are responsible for the spin-flip transitions $\lambda_\gamma \to \lambda_\phi = 0$ and generate a finite value for ρ^0_{00}. The contribution of the second term is dominant, and it can be estimated as

$$\rho^0_{00} \simeq \frac{k^2_\gamma (|t| + 2p^2_x)}{\overline{s^2}},$$

$$\overline{s^2} = (s - M^2_N)^2 \left(1 - \frac{M^2_\phi + |t|}{s - M^2_N} \right). \tag{50}$$

This equation shows that ρ^0_{00} increases monotonically with increasing $|t|$, and $E_\gamma = 2.2$ GeV and at $\theta = \pi$, it reaches large value of $\rho^0_{00} \simeq 0.6$.

The interaction of the photon spin with the orbital momentum is responsible for the so-called double spin-flip transition $\lambda_\gamma \to \lambda_\phi = -\lambda_\gamma$ and generates $\rho^0_{1\text{-}1}$, which is defined by the interference of the first and third terms in Eq. (49),

$$\rho^0_{1-1} \simeq \frac{p^2_x (M^2_\phi + |t|)}{\overline{s^2}}. \tag{51}$$

This matrix element reaches its maximum value $\rho^0_{1-1} \simeq 0.2$ at $|t| \simeq 1$ GeV^2 and $E_\gamma = 2.2$ GeV. Note that this matrix element depends on the choice of the gauge parameter $\bar{p} = ap$

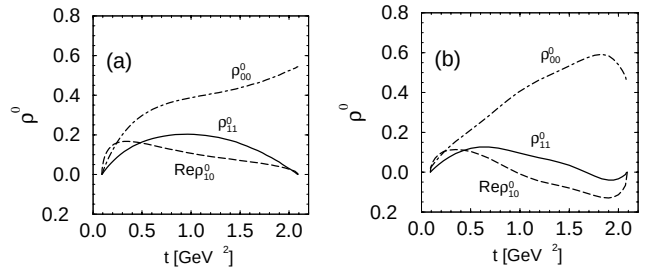

FIG. 6. Spin-density matrix elements ρ^0_{00}, ρ^0_{10}, and $\rho^0_{1\text{-}1}$ for the reaction $\gamma p \to \phi p$ as a function of $-t$ at $E_\gamma = 2.2$ GeV shown as dot-dashed, solid, and dashed lines, respectively. (a) Result for the Pomeron-exchange amplitude; (b) result for the full model.

$+bp'$ in Eq. (28) with constrains $a,b>0$ and $a+b=1$, which provide the proper high-energy limit. Our choice is $a=b=\frac{1}{2}$. $\rho^0_{1\text{-}1}$ is proportional to $\varepsilon_\lambda(\gamma)\cdot\bar{p}/[s-M_N^2-b(M_\phi^2+|t|)]$. Since in the GJ system $p_x=p'_x$, thus the product $\varepsilon_\lambda(\gamma)\cdot\bar{p}=\sqrt{2}\lambda p_x$ does not depend on this choice. The rest dependence on choice of $\bar{p}$ is rather weak. Thus, at $E_\gamma = 2.2$ GeV the choice of $a=1,b=0$ ($a=0,b=1$) results in the decrease (increase) of $\rho^0_{1\text{-}1}$ by a factor of 20%.

The resonant channel and f'_2 trajectory [first and third terms in the brackets in Eq. (38b)] also generate the finite spin-flip matrix elements, but in the region with $|t|<1$ GeV^2 their contribution to $\rho^0_{00}, \rho^0_{1\text{-}1}$ is about of an order of magnitude smaller than the contribution from the Pomeron-exchange amplitude of Eq. (49). At large momentum transfers with $|t|\sim|t|_{\max}$, the resonant channel becomes essential.

In Fig. 6 we show the t dependence of the three ρ^0 matrix elements at $E_\gamma = 2.2$ GeV. ρ^0 defines the angular distribution of K^+K^- mesons in reactions with unpolarized photons [Eqs. (10) and (14)]. Figure 6(a) is for the pure Pomeron-exchange amplitude [Eq. (23)] and Fig. 6(b) for the full model which includes diffractive part, PS meson-exchange, and resonance excitations. One can see that for the full model the nonzero values of these spin-density matrix elements at forward-angle photoproduction, ($|t|<1$ GeV^2) are mostly determined by the Pomeron-exchange contribution. At large momentum transfers the resonant excitations play a key role.

The one-dimensional angular distributions $W^0(\cos\Theta)$ and $W^0(\Phi)$ at three values of $|t|=0.2$, 0.5, and 1.8 GeV^2 are shown in Figs. 7(a) and 7(b), respectively. For small momentum transfers ($|t|\lesssim 0.2$ GeV^2), the ϕ mesons are produced transversely with its spin aligned along the quantization axis $\mathbf{z}'$ ($\rho^0_{00}\ll 1$). This results in the angular distribution $W^0(\cos\Theta)\simeq\sin^2\Theta$. When $|t|$ increases, the spin-flip processes generate longitudinally polarized ϕ mesons (ρ^0_{00} becomes finite). Initially, this leads to depolarization of the ϕ mesons with $W^0(\cos\Theta)\simeq 0.5$ at $|t|\sim 0.5$–0.6 GeV^2, and then, at large momentum transfers, to a predominance of the longitudinal polarization with $W^0(\cos\Theta)\simeq a+b\cos^2\Theta$, where $a,b>0$.

The Φ dependence of W^0 is determined completely by the double-spin-flip processes. The amplitude of the azimuthal-

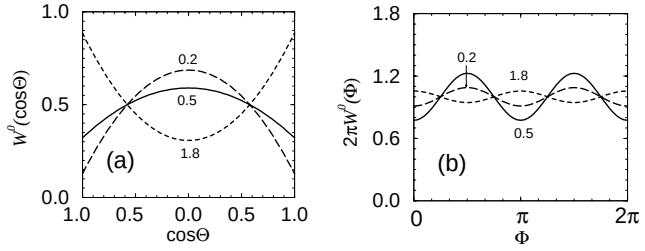

FIG. 7. The angular distribution of the ϕ-meson decay in the reaction $\gamma p \to \phi p$ with unpolarized photon beam at $E_\gamma = 2.2$ GeV and $|t|=0.2$, 0.5, and 1.8 GeV^2. (a) The dependence on $\cos\Theta$ (integrated over the azimuthal angle Φ); (b) the dependence on Φ (integrated over $\cos\Theta$).

angle modulation is proportional to $2\rho^0_{1\text{-}1}$. It is exactly zero at $\theta=0$ ($|t|=|t|_{\min}$), increases with increasing $|t|$, and reaches its maximum value at $|t|\simeq 0.6$ GeV^2. It goes down at large momentum transfers, as it is shown in Fig. 7(b). It is important to note that the spin-conserving scalar- and pseudoscalar-exchange processes do not contribute to $\rho^0_{1\text{-}1}$. The contribution of the tensor part of f'_2 [square brackets in Eq. (38b)] and the resonant channel at $|t|\lesssim 0.8$ GeV^2 are rather small. Therefore, the distribution $W^0(\Phi)$ may be used as a tool to study dynamics of the spin-orbital interaction generated by the gluon-exchange processes in diffractive amplitude. At large momentum transfers, $W^0(\cos\Theta)$ and $W^0(\Phi)$ are sensitive to the resonant channel.

Figure 8 displays the energy dependence of the matrix elements ρ^0_{00} and $\rho^0_{1\text{-}1}$ which define the one-dimensional distributions $W^0(\cos\Theta)$ and $W^0(\Phi)$, respectively, at fixed $|t|$; $|t|=0.4$ GeV^2. The left (a) and right (b) panels correspond to calculation for the Pomeron exchange and for the full amplitudes, respectively. One can see that the energy dependence of the matrix elements in both cases is very similar to each other. The increase of ρ^0_{00} with increasing energy reflects a definite increase of the amount of the longitudinally polarized ϕ mesons with energy. The increase of $\rho^0_{1\text{-}1}$ with energy results in increasing the amplitude of the Φ modulation in $W(\Phi)$.

Figures 9 and 10 display the t dependence of the matrix elements of ρ^1 and ρ^2 matrices, respectively. These matrix elements represent the angular distribution of K^+K^- mesons in reactions with the linearly polarized photons [cf. Eqs. (12) and (17)]. Notation is the same as in Fig. 6. Consider first the

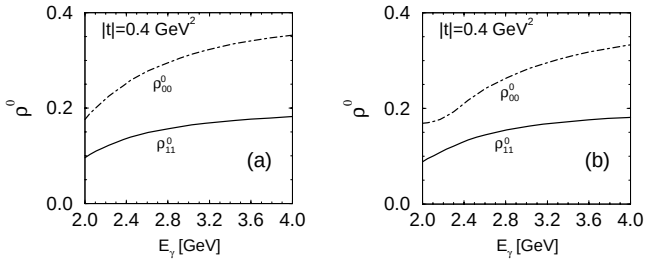

FIG. 8. Spin-density matrix elements ρ^0_{00} and $\rho^0_{1\text{-}1}$ for the reaction $\gamma p \to \phi p$ as a function of E_γ at $|t|=0.4$ GeV^2. (a) Result for the Pomeron-exchange amplitude; (b) result for the full model.

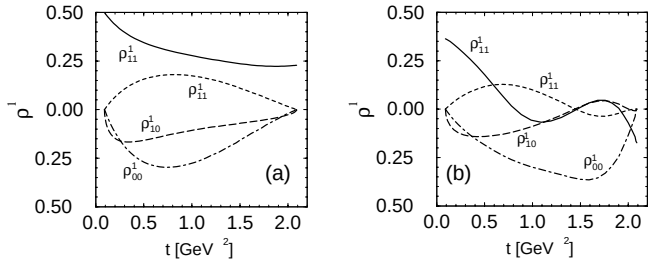

FIG. 9. Spin-density matrix elements ρ^1_{00}, ρ^1_{11}, ρ^1_{10}, and $\rho^1_{1\text{-}1}$ for the reaction $\gamma p \to \phi p$ as a function of $-t$ at $E_\gamma = 2.2$ GeV. (a) Result for the Pomeron-exchange amplitude; (b) result for the full model.

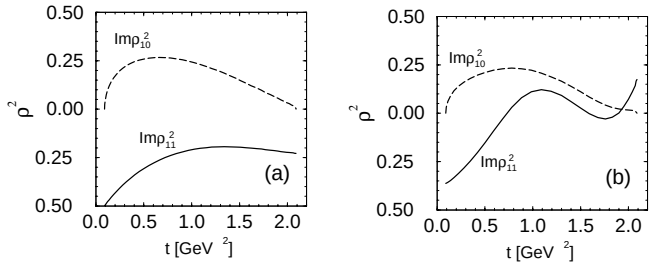

FIG. 10. Spin-density matrix elements $\mathrm{Im}\,\rho^2_{10}$ and $\mathrm{Im}\,\rho^2_{1\text{-}1}$ for the reaction $\gamma p \to \phi p$ as a function of $-t$ at $E_\gamma = 2.2$ GeV. (a) Result for the Pomeron-exchange amplitude; (b) result for the full model.

matrix element $\rho^1_{1\text{-}1}$. In the case of the helicity-conserving model of Eq. (49), its meaning is the asymmetry in the contribution from natural- and unnatural-parity-exchange parts,

$$\rho^1_{1\text{-}1} = \frac{1}{2}\,\frac{|I_0^{\mathrm{N}}|^2 - |I_0^{\mathrm{U}}|^2}{|I_0^{\mathrm{N}}|^2 + |I_0^{\mathrm{U}}|^2}. \tag{52}$$

Therefore, it is considered as a good tool to extract the relative contributions of the unnatural-parity-exchange processes from the angular distribution $W^L(\Phi - \Psi)$. However, the existence of spin-flip processes violates this identity, and instead of Eq. (52) one has to use

$$\rho^1_{1\text{-}1} = \frac{1}{2}\,\frac{|I_0^{\mathrm{N}}|^2 - |I_0^{\mathrm{U}}|^2 + |I_1^{1-1}|^2}{|I_0^{\mathrm{N}}|^2 + |I_0^{\mathrm{U}}|^2 + |I^{10}|^2 + |I_2^{1-1}|^2}, \tag{53}$$

where $|I^{10}|^2 = \mathrm{Tr}[I_{\alpha;10} I^\dagger_{\alpha;10}]$ is the spin contribution for transitions $\lambda_\gamma \to \lambda_\phi = 0$; $|I_1^{\alpha;1-1}|^2 = \mathrm{Tr}[I_{\alpha;1\text{-}1} I^\dagger_{\alpha;-11}]$ and $|I_2^{\alpha;1-1}|^2 = \mathrm{Tr}[I_{\alpha;1\text{-}1} I^\dagger_{\alpha;1\text{-}1}]$ are the spin-flip contributions for transitions $\lambda_\gamma \to \lambda_\phi = -\lambda_\gamma$. Only at $\theta = 0$ ($|t| = |t|_{\min}$) and $\rho^0_{00} \simeq 0$, Eqs. (52) and (53) are equivalent to each other.

For the pure Pomeron-exchange amplitude, the contribution of the double spin flip can be estimated as

$$\frac{1}{N}|I_1^{1\text{-}1}|^2 \simeq \frac{1}{N}|I_2^{1\text{-}1}|^2 \simeq \frac{1}{2(1-\rho^0_{00})}(\rho^0_{1\text{-}1})^2 \ll \rho^0_{00}, \tag{54}$$

where N is the normalization factor, defined by Eq. (7). Therefore, for the pure Pomeron-exchange amplitude we get the relation

$$\rho^1_{1\text{-}1} \simeq \frac{1}{2}(1 - \rho^0_{00}), \tag{55}$$

which is confirmed by the explicit calculation of ρ^0_{00} and $\rho^1_{1\text{-}1}$, see in Figs. 6(a) and 9(a), $\rho^1_{1\text{-}1}$ decreases from $\frac{1}{2}$ at $|t| = |t|_{\min}$ to 0.23 at $|t| = |t|_{\max}$.

For the forward-angle photoproduction, where the contribution of the resonant channel to $|I^{1\text{-}1}|^2$ remains negligible, we get the following relation between $\rho^1_{1\text{-}1}$ and the relative contribution of the spin-conserving unnatural-parity-exchange amplitude,

$$|\alpha^U|^2 \simeq \frac{|I_0^{\mathrm{U}}|^2}{|I_0^{\mathrm{N}}|^2 + |I_0^{\mathrm{U}}|^2 + |I^{10}|^2}, \tag{56}$$

which can be rewritten as

$$|\alpha^U|^2 \simeq \frac{1}{2}(1 - 2\rho^1_{1\text{-}1} - \rho^0_{00}). \tag{57}$$

This means that for evaluation of the relative contribution of the unnatural-parity exchange part from the data with a linearly polarized beam at small momentum transfers, one has to account for ρ^0_{00}, which in turn is extracted from the analysis of $W^0(\cos\Theta)$. At large $|t|$, $\rho^1_{1\text{-}1}$ is determined by the interplay between the resonant and all other channels and has no simple meaning.

Using the definition of spin-density matrices in Eq. (6), one can get the following relation:

$$-\mathrm{Im}\,\rho^2_{1\text{-}1} \simeq \rho^1_{1\text{-}1} - \frac{[\rho^0_{1\text{-}1}]^2}{1-\rho^0_{00}}. \tag{58}$$

Therefore, in Eq. (15), $\overline{\rho^1_{1\text{-}1}} \simeq \rho^1_{1\text{-}1}$ and $\Delta_{1\text{-}1} \simeq 0$. So, the term proportional to $\cos[2(\Phi + \Psi)]$ in Eq. (15) is negligible.

Figure 11(a) shows the angular distribution $W^L(\Phi - \Psi)$ at $|t| = 0.2$, 0.5, and 1.8 GeV^2 ($E_\gamma = 2.2$ GeV). The amplitude of modulation of this distribution is equal to $2P_\gamma \rho^1_{1\text{-}1}$. In calculation we use $P_\gamma = 0.95$, which is reasonable for the highly polarized photon beam at the LEPS of SPring-8 [61].

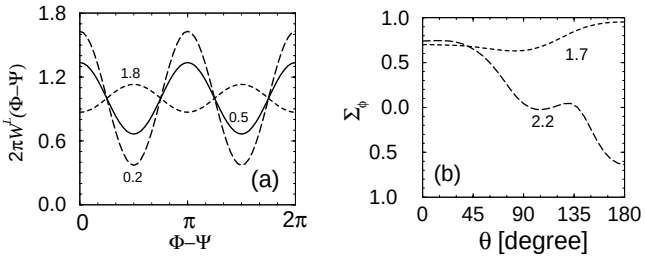

FIG. 11. (a) The angular distribution of the ϕ-meson decay as a function of Φ-Ψ in the reaction $\gamma p \to \phi p$ with linearly polarized photon beam at $E_\gamma = 2.2$ GeV and $-t = 0.2$, 0.5, and 1.8 GeV^2; (b) the ϕ-meson-decay asymmetry for $\gamma p \to \phi p$ reaction at $E_\gamma = 1.7$ and 2.2 GeV.

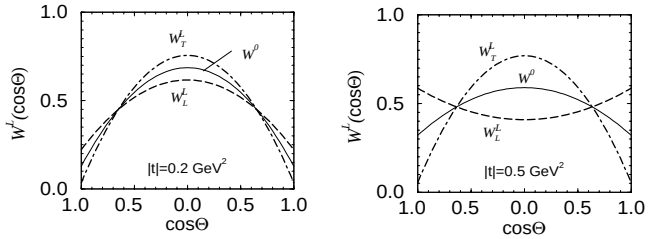

FIG. 12. The ϕ-meson-decay distribution in the reaction $\gamma p \to \phi p$ with linearly polarized photon beam at $E_\gamma = 2.2$ GeV for vertical beam polarization with $\Psi = (\pi/2)$ (W_T^L) and horizontal polarization with $\Psi = 0$ (W_L^L) at $|t| = 0.2$ (a) and 0.5 GeV^2 (b).

The amplitude of modulation has a maximum value at forward angles and decreases with increasing $|t|$.

Figure 11(b) displays the ϕ-meson-decay asymmetry Σ_ϕ (20), as a function of the production angle θ. It is determined by the matrix elements $\rho^{1,0}_{1\text{-}1}$ and $\rho^{1,0}_{11}$. For the pure helicity-conserving amplitude there exist an identity $\Sigma_\phi = 2\rho^1_{1\text{-}1}$. But in spin-flip processes, this relation is violated. The scale of the violation increases with increasing $|t|$. At large $|t|$, the shape of Σ_ϕ is sensitive to the resonant amplitude.

The decay distribution as a function of $\cos\Theta$ for the linearly polarized beam depends on the beam-polarization angle Ψ and matrix elements ρ^1_{11} and ρ^1_{00} [cf. Eq. (15)]. In Fig. 12, we show results for the calculation of $W_L^L(\cos\Theta) \equiv W^L(\cos\Theta, \Psi = 0)$ and $W_T^L(\cos\Theta) \equiv W^L(\cos\Theta, \Psi = \pi/2)$ at $|t| = 0.2$ GeV^2 and $|t| = 0.5$ GeV^2: left (a) and right (b) panels, respectively. Also, for comparison, results for the angular distributions with an unpolarized beam are shown (thin solid lines). The difference between W_L^L and W_T^L disappears at $|t| \simeq |t|_{\min}$, but becomes very large at finite $|t|$. Using these distributions, one can extract ρ^1_{00} and ρ^1_{11} from the data:

$$\rho^1_{00} = \frac{1}{3P_\gamma}[W_T^L(\Theta = 0) - W_L^L(\Theta = 0)],$$

$$\rho^1_{11} = \frac{1}{3P_\gamma}\left[W_T^L\left(\Theta = \frac{\pi}{2}\right) - W_L^L\left(\Theta = \frac{\pi}{2}\right)\right]. \tag{59}$$

The decay distribution as a function of the beam-polarization angle Ψ is defined by the matrix elements ρ^1_{11} and ρ^1_{00}. These matrix elements, taken separately, are finite at $|t| \neq |t|_{\min}, |t|_{\max}$. But the absolute value of the sum $2\rho^1_{11} + \rho^1_{00}$ in Eqs. (18) is very small at forward-angle photoproduction,

$$2\rho^1_{11} + \rho^1_{00} \simeq 0, \tag{60}$$

and becomes sizable only at large momentum transfers. Equation (60) allows us to express the angular distribution for the linearly polarized beam $W^L(\cos\Theta, \Psi)$ similar to the distribution for unpolarized beam $W^0(\cos\Theta)$,

$$W^L(\cos\Theta, \Psi) = \frac{3}{2}\left(\frac{1}{2}(1 - \rho^{\text{eff}}_{00})\sin^2\Theta + \rho^{\text{eff}}_{00}\cos^2\Theta\right), \tag{61}$$

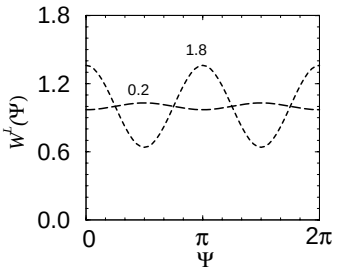

FIG. 13. The total ϕ-meson-decay distribution in the reaction $\gamma p \to \phi p$ with linearly polarized photon beam at $E_\gamma = 2.2$ GeV and $-t = 0.2$ and 1.8 GeV^2 as a function of the angle between the beam polarization and production planes.

where

$$\rho^{\text{eff}}_{00} = \rho^0_{00} - P_\gamma \rho^1_{00}\cos(2\Psi). \tag{62}$$

Figure 13 shows the calculation of the total decay distribution as a function of the beam polarization angle Ψ. It is defined by the sum $2\rho^1_{11} + \rho^1_{00}$ [cf. Eq. (18)], which is finite only at large momentum transfers. Here the sign and the amplitude of $W^L(\Psi)$ is determined by the resonant channels and prediction in this region is sensitive to the underlying theoretical model for the resonance part. The beam asymmetry Σ_x of Eq. (4) is related to $W^L(\Psi)$ as

$$\Sigma_x = \frac{W^L\left(\frac{\pi}{2}\right) - W^L(0)}{W^L\left(\frac{\pi}{2}\right) + W^L(0)}, \tag{63}$$

and for the pure Pomeron exchange channel is defined by the interference of the first and third terms in Eq. (30) and can be evaluated in the c.m. system as

$$\Sigma_x \simeq \frac{q^2\sin^2\theta}{2s}. \tag{64}$$

It is positive and increases near threshold with energy as q^2 (proportional to increase of the phase space), but remains small: $\Sigma_x \ll 1$. For the full model, the dominant contribution to Σ_x at large $|t|$ comes from the resonant channel. Thus, at $|t| \sim 1.8$ GeV ($E_\gamma = 2.2$ GeV), Σ_x tends to be negative with large absolute value. This is illustrated in Fig. 14 where we

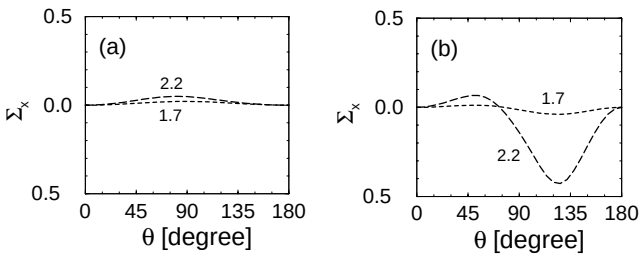

FIG. 14. The beam asymmetry for $\gamma p \to \phi p$ reaction at $E_\gamma = 1.7$ and 2.2 GeV. (a) Result for the Pomeron-exchange channel; (b) result for the full model.

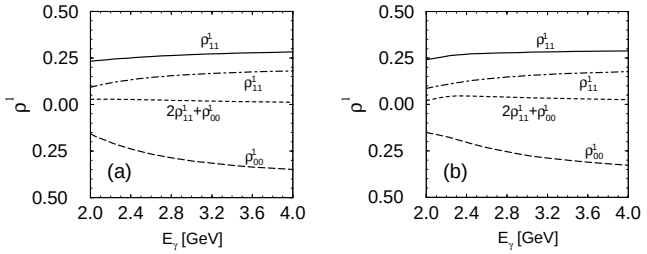

FIG. 15. Spin-density matrix elements ρ^1_{00}, ρ^1_{11}, ρ^1_{1-1}, and sum of $2\rho^1_{11}+\rho^1_{00}$ for the reaction $\gamma p \to \phi p$ as a function of E_γ at $|t| = 0.4$ GeV^2. (a) Result for the Pomeron-exchange amplitude; (b) result for the full model.

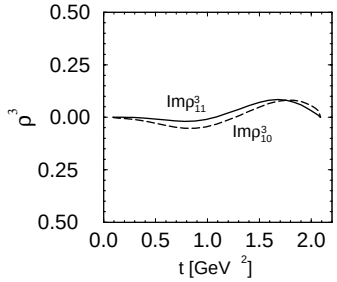

FIG. 16. Spin-density matrix elements $\mathrm{Im}\,\rho^3_{10}$ and $\mathrm{Im}\,\rho^3_{1-1}$ for the reaction $\gamma p \to \phi p$ as a function of $-t$ at $E_\gamma = 2.2$ GeV for the full model.

show Σ_x, calculated for the pure Pomeron-exchange amplitude and for the full model at the left (a) and the right (b) panels, respectively.

Figure 15 displays the energy dependence of the most important matrix elements, which define the angular distributions of $\phi \to K^+K^-$ decay with the linearly polarized photon beam and the beam asymmetry. The left (a) and right (b) panels correspond to the calculation for the Pomeron exchange and for the full amplitudes, respectively. The energy dependence of ρ^1_{00} and ρ^1_{11} in both cases is similar to each other. The difference in ρ^1_{1-1} is explained by the contribution of unnatural parity π-η meson exchange in the total amplitude. The calculation results in some decrease of ρ^1_{1-1} and ρ^0_{11}; increase of ρ^1_{11}, and almost constant value for $2\rho^1_{11} + \rho^1_{00} \simeq 0$.

Unfortunately, the available experimental data on the spin-density matrix elements $\rho^{1,2}$ in ϕ-meson photoproduction at $E_\gamma \sim 2$–5 GeV [57] are of a pure accuracy to make some definite conclusion about the photoproduction mechanism. To increase statistics they are combined at two energies (2.8 and 4.7 GeV) with momentum transfers $0.02 \leqslant |t| \leqslant 0.8$ GeV^2. The data are given in helicity frame where the spin-density matrix elements have additional kinematical dependence on the momentum transfers compared to the GJ system [20]. In Table I we show the comparison of this data with our calculation for the ''central'' point $E_\gamma = 3.75$ GeV and $|t| = 0.4$ GeV^2 in the helicity frame. One can see that the theoretical values are within experimental accuracy. The exception is ρ^1_{1-1}, where the calculated value (0.44) exceeds the experimental one (0.18 ± 0.13) by two standard deviations. But close inspection shows some inconsistency with the data. Really, following the identity of Eq. (58) and using experimental values of $\rho^0_{00}, \rho^0_{1-1}$, one could expect $\rho^1_{1-1} \sim -\mathrm{Im}\rho^2_{1-1}$; i.e., it must be close to 0.5, which is also supported by Fig. 29 of Ref. [57]. Nevertheless, it is clear that for better understanding of details of the photoproduction processes the more precise experimental data in a wide kinematical region are desired.

TABLE I. Comparison of calculated spin-density matrix elements in helicity system with experimental data of Ref. [57] at $E_\gamma = 2.8$ and 4.7 GeV for $0.02 \leqslant |t| \leqslant 0.8$ GeV^2. Theoretical prediction is done at $E_\gamma = 3.75$ and for $|t| = 0.4$ GeV^2.

$\rho_{\lambda\lambda'}$	Expt.	Calc.
ρ^0_{00}	-0.04 ± 0.06	0.061
$\mathrm{Re}\,\rho^0_{10}$	-0.00 ± 0.06	-0.067
ρ^0_{1-1}	-0.04 ± 0.10	0.042
ρ^1_{00}	-0.13 ± 0.09	0.010
ρ^1_{11}	-0.06 ± 0.11	0.018
$\mathrm{Re}\,\rho^1_{10}$	0.00 ± 0.09	0.063
ρ^1_{1-1}	0.18 ± 0.13	0.44
$\mathrm{Im}\,\rho^2_{10}$	-0.02 ± 0.10	-0.052
$\mathrm{Im}\,\rho^2_{1-1}$	-0.51 ± 0.16	-0.44

The spin-density matrix elements ρ^3, responsible for the angular distribution with the circularly polarized beam are shown in Fig. 16. They reach their maximum values $\mathrm{Im}\,\rho^3_{1-1(10)} \simeq 0.1$ at $|t| \sim 1.8$ GeV^2. The finite value of $\mathrm{Im}\,\rho^3_{1-1}$ generates an additional term in the angular distribution according to Eq. (19): $\Delta W^\pm(\Phi) = \pm(P_\gamma/\pi)\,\mathrm{Im}\,\rho^3_{1-1}\sin 2\Phi$. At forward photoproduction angles this term is rather weak and $W^\pm(\Phi) \simeq W^0(\Phi)$.

Next, we investigate the beam-target asymmetry which may be studied in reactions with a circularly polarized beam and polarized target. Using the notation of Eq. (5), the expression for helicity-conserving amplitudes (49), and neglecting spin-flip processes, we can estimate C_{BT} at forward-angle photoproduction as

$$C_{BT}(t_{\max}) \simeq 2|\alpha^U|\cos(\delta_N - \delta_U), \tag{65}$$

where δ_N, δ_U are the phases of the natural- and unnatural-parity exchange amplitudes, respectively. From this expression it seems quite reasonable to use C_{BT} as a tool for study-

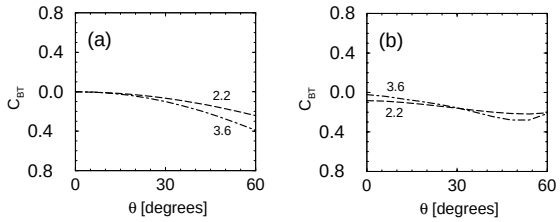

FIG. 17. The beam-target asymmetry for $E_\gamma = 2.2$ and 3.6 GeV at forward photoproduction angles. (a) Result for the Pomeron-exchange amplitude; (b) result for the full model.

ing contribution from exotic processes with unnatural-parity exchange, because the asymmetry depends on α^U, and not on $|\alpha^U|^2$ [37].

However, analysis of the pure Pomeron-exchange amplitude shows that the second term of Eq. (30) gives some contribution to C_{BT} even without admixture of an unnatural-parity exchange component. This term contains a part which describes the interaction of the photon and proton spins, which is governed by condition

$$\mathbf{s}_p + \boldsymbol{\lambda}_\gamma = \mathbf{s}_{p'}, \tag{66}$$

and select the initial state with the total spin $|\mathbf{s}_i| = \frac{1}{2}$. As a result, the beam-target asymmetry has an additional contribution,

$$\Delta C_{BT} \simeq -\frac{(E_p + M_N)(E_{p'} + M_N)(n - n'\cos\theta)^2 [q(M_\phi^2 + |t|^2 + kM_\phi)]^2}{4\overline{s^2}[M_\phi(E_\phi + M_\phi)]^2},$$

$$n = \sqrt{\frac{E_p - M_N}{E_p + M_N}}, \quad n' = \sqrt{\frac{E_{p'} - M_N}{E_{p'} + M_N}}. \tag{67}$$

Fortunately, at $E_\gamma = 2-3$ GeV and for $|t| \simeq |t|_{\min}$ this term is small and disappears with increasing E_γ. However, it is quite large at large momentum transfers. This is illustrated in Fig. 17 where we show calculations for the Pomeron-exchange amplitude and for the full model for $E_\gamma = 2.2$ and 3.6 GeV. At small $|t|$ and $E_\gamma \sim 2-3$ GeV, the conventional processes considered above do not contribute to C_{BT}; and it may be used as a tool to study the nondiffractive component with unnatural parity exchange, such as $s\bar{s}$ knockout [37], etc. At large $|t|$ the beam-target asymmetry is defined by the interplay of all channels and is very sensitive to the production mechanism.

V. SUMMARY

In this paper we have discussed several topics of current interest for the ϕ-meson photoproduction at low energies. In particular, we found that the spin-dependent interaction in the diffractive (Pomeron-exchange) amplitude is responsible for the spin-flip transitions which are suppressed completely in the helicity-conserving processes. These transitions give sizable contributions to the spin-density matrix elements and may be measured via the angular distributions of K^+K^- decays in reactions with unpolarized and polarized photons. Of special interest is the finite and large value of the $\rho^0_{1\text{-}1}$ matrix element generated by the double spin-flip transition. It is caused by the spin-orbital interaction inherent to the two-gluon exchange processes in the diffractive channel. This matrix element generates the Φ dependence of the decay-angular distribution in reactions with unpolarized photons at forward angles. That is, the spin observables at small $|t|$ may be used as a tool for studying diffractive mechanism in detail.

A combined study of ϕ and ω photoproduction at large angles allows the analysis of the status of OZI rule for ϕNN^* interactions relative to the standard estimation based on the violation of $\phi - \omega$ mixing from its ideal value. We found a large (factor of 4) scale of this violation, which agrees with other independent indications for this effect.

We have also shown that spin observables at large momentum transfers are due to the interplay between the resonant and all other channels, and therefore, may be used to test the resonance excitation mechanism, which is a issue of current interest.

It would be interesting to extend our analysis of spin-density matrix elements to the ω photoproduction too. This needs to include into consideration additional channels such as initial and final state interactions [55], direct quark exchange [54], contribution of the conventional meson trajectories [21], and others. This will be a subject of future study.

Another interesting problem we have not investigated in this work is to use the spin observables to extract information about the exotic isoscalar processes, such as $s\bar{s}$ knockout [34,37], G poles [24], etc., with unnatural-parity exchange properties. The most challenging question is to exclude the contribution of the pseudoscalar π-meson exchange. This problem may be solved in a combined study of the spin-density matrix elements measured using linearly polarized photons and the beam-target and/or beam-recoil double polarizations measured using circularly polarized photons on the proton and deuteron targets [62]. It is then possible to determine the absolute value and the phase of the ''exotic channel.'' The corresponding theoretical estimations will be presented in our forthcoming paper.

ACKNOWLEDGMENTS

We thank W.-C. Chang, S. Date, H. Ejiri, M. Fujiwara, K. Hicks, T. Hotta, K. Mawatari, T. Mibe, N. Muramatsu, T. Nakano, D. J. Tedeschi, and R. G. T. Zegers for fruitful discussions. This work was supported in part by the U.S. Department of Energy, Nuclear Division, Contract No. W-31-109-ENG-38.

APPENDIX: COMPARISON STUDIES OF DIFFRACTIVE MECHANISMS

Up to now we have discussed diffractive photoproduction, where the dominance contribution comes from the Pomeron exchange, and the additional trajectories are added to im-

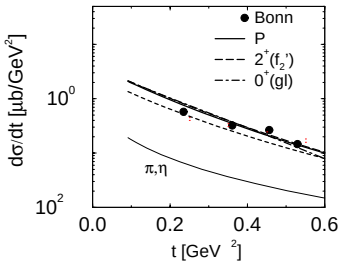

FIG. 18. (a) The differential cross section of the $\gamma p \to \phi p$ reaction at $E_\gamma = 2.2$ GeV for the models "P," "2^+," and "0^+" indicated by solid, dashed, and dot-dashed curves, respectively. The contribution of the pseudoscalar π, η exchange is shown by the solid thin curve. The short dashed curve corresponds to the case where the diffractive channel represents Pomeron and PS exchange. Data are taken from Ref. [63].

prove the total unpolarized cross section at low energy. Let us denote this diffractive model as a model "*P*." As we discussed in Sec. III the finite value of threshold parameter $a_P \sim s_P$ in Eq. (40) eliminates the Pomeron contribution at $E_\gamma \sim 2$ GeV, which must be compensated by an increase of strength of the additional trajectories. The validity of different assumptions must be checked in study of the polarization observables in diffractive region, because the vertex functions for the Pomeron and other trajectories in Eqs. (27)–(38b) lead to different predictions. By way of illustration, we shall compare the model *P* with the model "2^+," which represents the f_2' Regge trajectory and PS-meson exchange, and the model "0^+," which is the PS meson exchange and the scalar (glueball exchange) trajectory. The last two cases are realized if one chooses the threshold parameters in Eq. (40) as $a_P \simeq s_R \sim (M_N + M_\phi)^2$ and $a_{R \neq P} = 0$.

In Fig. 18, we show the differential cross section of the $\gamma p \to \phi p$ reaction as a function of $-t$ at $E_\gamma = 2.2$ GeV for the three models together with the available experimental data [63]. Parameters of the Pomeron exchange amplitude are fixed from the high energy region, for other trajectories we use $g_{2^+} = 0.82\, g_P$, and $g_{0^+} = 3.9\, g_P$. The contribution of the pseudoscalar π, η exchange is also shown for completeness. We also show case when the diffractive channel is built from the Pomeron and PS exchanges. In this case the calculation is slightly below data. But all other three models are close to each other and it is difficult to distinguish between them using only unpolarized differential cross section. The situation reverses if we look at spin observables.

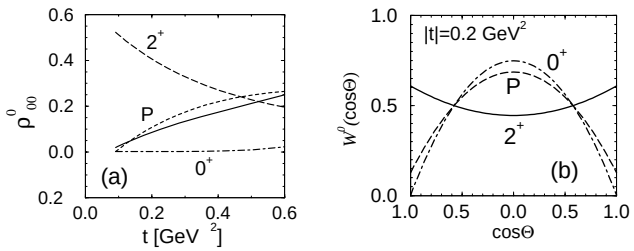

FIG. 19. The spin-density matrix element ρ^0_{00} (a) and the angular distribution $W^0(\cos\Theta)$ (b) for the three models of diffractive ϕ-meson photoproduction. Notation is the same as in Fig. 18.

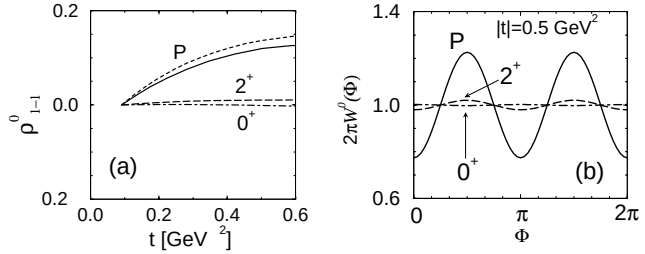

FIG. 20. The spin-density matrix element $\rho^0_{1\text{-}1}$ (a) and the angular distribution $W^0(\Phi)$ (b) for the three models of diffractive ϕ-meson photoproduction. Notation is the same as in Fig. 18.

Figure 19(a) shows ρ^0_{00} for different models as a function of $-t$ at $E_\gamma = 2.2$ GeV. Thus, for the 0^+ exchange, $\rho^0_{00} \simeq 0$, and for the Pomeron exchange, it increases monotonically with $|t|$. For the 2^+ exchange ρ^0_{00} decreases with *t*, starting from a large value at $|t| = |t|_{\min}$, because of the spin-flip terms. They are the first and the third terms in the square brackets of Eq. (38b). These terms generate a finite value of ρ^0_{00} even at forward-angle photoproduction. The difference in ρ^0_{00} leads to the difference in decay distribution $W^0(\cos\Theta)$ shown in Fig. 19(b) for $|t| = 0.2$ GeV^2. For 0^+ exchange ϕ mesons produced to be transversely polarized, the Pomeron-exchange process results in partial ϕ-meson "depolarization." In case of 2^+ exchange we get rather strong ϕ-meson depolarization with an enhancement of the longitudinal polarization at $|t| = |t|_{\min}$. One can also see that the difference between the "hybrid" model *P* (solid curve) in Fig. 19(a) and pure Pomeron-exchange model (short dashed curve) is negligible.

In Fig. 20(a) we show $\rho^0_{1\text{-}1}$ generated by the double-spin-flip transition $\lambda_\gamma \to \lambda_\phi = -\lambda_\gamma$. This matrix element is proportional to interference of helicity-conserving and double spin-flip transition amplitudes, and is almost equal to zero for the 0^+ model. For *P* and 2^+ models it increases monotonically with increasing $|t|$, but in the 2^+ exchange it is much smaller.

As we have discussed above, the matrix element $\rho^1_{1\text{-}1}$ depends on the contribution of unnatural-parity exchange components and strength of the single-spin-flip component or ρ^0_{00} [cf. Eq. (57)]. In the 2^+ model the spin-conserving component or ρ^0_{11} is dominated by the PS exchange, and therefore

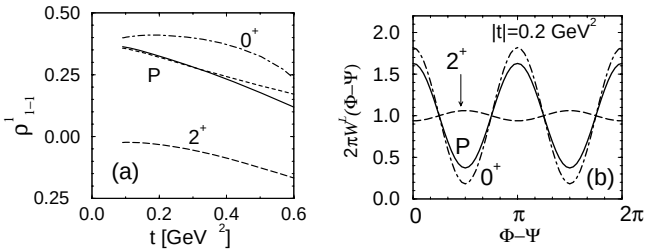

FIG. 21. The spin-density matrix element $\rho^1_{1\text{-}1}$ (a) and the angular distribution $W^L(\Phi - \Psi)$ (b) for the three models of diffractive ϕ-meson photoproduction with linearly polarized photons. Notation is the same as in Fig. 18.

the relative contribution of unnatural-parity exchange is smaller than in other cases. Also, ρ^0_{00} is greater. This leads to strong decreasing of $\rho^1_{1\text{-}1}$ at forward angles up to the negative values, which is illustrated in Fig. 21(a). At small and finite $|t|$, this matrix element is the biggest for 0^+ model, since there are no spin-flip processes in this case. The corresponding angular distributions $W^L(\Phi-\Psi)$ at $|t|=0.2$ GeV^2 are shown in Fig. 21(b). One can see strong difference between 2^+ exchange and other models. Existing data [57] support for the small value for ρ^0_{00} and finite value for $\rho^1_{1\text{-}1}$. This eliminates large a component of the 2^+ exchange. In order to distinguish between the Pomeron and 0^+ exchange, one needs at least data on $\rho^0_{1\text{-}1}$-matrix element (cf. Fig. 20), which is crucial for these models on the qualitative level.

[1] A. Donnachie and P.V. Landshoff, Phys. Lett. B **185**, 403 (1987); Nucl. Phys. **B244**, 322 (1984); **B267**, 690 (1986).
[2] P.V. Landshoff and O. Nachtmann, Z. Phys. C **35**, 405 (1987).
[3] S.V. Goloskokov, Phys. Lett. B **315**, 459 (1993).
[4] J.-M. Laget and R. Mendez-Galain, Nucl. Phys. **A581**, 397 (1995).
[5] M.A. Pichowsky and T.-S.H. Lee, Phys. Lett. B **379**, 1 (1996); Phys. Rev. D **56**, 1644 (1997).
[6] A. Hebecker and P.V. Landshoff, Phys. Lett. B **419**, 393 (1998).
[7] J.R. Cudell, K. Kang, and S.K. Kim, Phys. Lett. B **395**, 311 (1997).
[8] L.D. Solovev, Teor. Mat. Fiz. **126**, 247 (2001) [Theor. Math. Phys. **126**, 203 (2001)].
[9] Q. Zhao, Z. Li, and C. Bennhold, Phys. Lett. B **436**, 42 (1998); Phys. Rev. C **58**, 2393 (1998).
[10] Q. Zhao, J.P. Didelez, M. Guidal, and E. Hourany, Nucl. Phys. **A684**, 351 (2001).
[11] Q. Zhao, Phys. Rev. C **63**, 025203 (2001).
[12] M. Post and U. Mosel, Nucl. Phys. **A688**, 808 (2001).
[13] Yongseok Oh, A. Titov, and T.-S.H. Lee, Phys. Rev. C **63**, 025201 (2001).
[14] Q. Zhao, B. Saghai, and J.S. Al-Khalili, Phys. Lett. B **509**, 231 (2001); Q. Zhao, nucl-th/0202023.
[15] M.F.M. Lutz, Gy. Wolf, and B. Friman, Nucl. Phys. **A706**, 431 (2002).
[16] A.I. Titov and T.-S.H. Lee, Phys. Rev. C **66**, 015204 (2002).
[17] N. Isgur and G. Karl, Phys. Lett. **72B**, 109 (1977); Phys. Rev. D **18**, 4187 (1978); **19**, 2653 (1979); R. Koniuk and N. Isgur, *ibid.* **21**, 1868 (1980).
[18] S. Capstick, Phys. Rev. D **46**, 2864 (1992).
[19] S. Capstick and W. Roberts, Phys. Rev. D **49**, 4570 (1994).
[20] A.I. Titov, T.-S.H. Lee, H. Toki, and O. Streltsova, Phys. Rev. C **60**, 035205 (1999).
[21] J.-M. Laget, Phys. Lett. B **489**, 3133 (2000).
[22] R.A. Williams, Phys. Rev. C **57**, 223 (1998).
[23] T. Nakano and H. Toki, in *Proceedings of the International Workshop on Exiting Physics and New Accelerator Facilities, Hyogo, 1997*, edited by H. Toki and S. Date (World Scientific, Singapore, 1998), p. 48.
[24] N.I. Kochelev and V. Vento, Phys. Lett. B **515**, 375 (2001); N.I. Kochelev, D.P. Min, V. Vento, and A.V. Vinnikov, Phys. Rev. D **65**, 097504 (2002).
[25] H. Genz and G. Hölner, Phys. Lett. **61B**, 389 (1976).
[26] R.L. Jaffer, Phys. Lett. B **229**, 275 (1989).
[27] S.B. Gerasimov, Phys. Lett. B **357**, 666 (1995); Chin. J. Phys. (Taipei) **34**, 848 (1996).
[28] S. Okubo, Phys. Lett. **5**, 165 (1963); G. Zweig, CERN Report No. 8182/TH 401; CERN Report No. 8419/TH 412 1964 (unpublished); J. Iizuka, Prog. Theor. Phys. Suppl. **37/38**, 21 (1966); G. Alexander, H.J. Lipkin, and P. Scheck, Phys. Rev. Lett. **17**, 412 (1966).
[29] J. Gasser, H. Leutwyler, and M.E. Sainio, Phys. Lett. B **253**, 252 (1991).
[30] ASTERIX Collaboration, J. Reifenrother *et al.*, Phys. Lett. B **267**, 299 (1991).
[31] Crystal Barrel Collaboration, V.G. Ableev *et al.*, Nucl. Phys. **A585**, 577 (1995).
[32] OBELIX Collaboration, A. Bertin *et al.*, Phys. Lett. B **388**, 450 (1996).
[33] J. Ellis, M. Karliner, D.E. Kharzeev, and M.G. Sapozhnikov, Nucl. Phys. **A673**, 256 (2000); J. Ellis, *ibid.* **A684**, 53 (2001).
[34] E.M. Henley, G. Krein, and A.G. Williams, Phys. Lett. B **281**, 178 (1992); E.M. Henley, T. Frederico, S.J. Pollock, S. Ying, G. Krein, and A.G. Williams, Few-Body Syst., Suppl. **6**, 66 (1992).
[35] M. Pichowsky, Ç. Şavkli, and F. Tabakin, Phys. Rev. C **53**, 593 (1996).
[36] A.I. Titov, Y. Oh, and S.N. Yang, Phys. Rev. Lett. **79**, 1634 (1997).
[37] A.I. Titov, Y. Oh, S.N. Yang, and T. Morii, Phys. Rev. C **58**, 2429 (1998); Nucl. Phys. **A684**, 354 (2001).
[38] Particle Data Group, K. Hagiwara *et al.*, Phys. Rev. D **66**, 010001 (2002).
[39] K. Schilling, K. Seyboth, and G. Wolf, Nucl. Phys. **B15**, 397 (1970).
[40] P.D.V. Collins, *An Introduction to Regge Theory & High Energy Physics* (Cambridge University Press, London, 1977).
[41] A. Donnachie and R.G. Kirsopp, Nucl. Phys. **B10**, 433 (1969).
[42] J.R. Cudell and I. Royen, Phys. Lett. B **397**, 317 (1997).
[43] M. Diehl, Eur. Phys. J. C **6**, 503 (1999).
[44] F.E. Low, Phys. Rev. D **12**, 163 (1975); S. Nussinov, Phys. Rev. Lett. **34**, 1286 (1975).
[45] J.R. Cudel, A. Donnachie, and P.V. Landshoff, Nucl. Phys. **B322**, 55 (1989).
[46] M.G. Ryskin, Z. Phys. C **57**, 89 (1993).
[47] B. Friman and M. Soyeur, Nucl. Phys. **A600**, 477 (1996).
[48] M. Guidal, J.M. Laget, and M. Vanderhaegen, Nucl. Phys. **A627**, 645 (1997).
[49] P.D.V. Collins and E.J. Squires, *Regge Poles in Particle Physics*, Springer Tracts in Modern Physics Vol. 45 (Springer-Verlag, Berlin, 1968).
[50] S.V. Talalov, hep-ph/010128.
[51] T. Sato and T.-S.H. Lee, Phys. Rev. C **54**, 2660 (1996).
[52] M. Benmerrouche, N.C. Mukhopadhyay, and J.F. Zhang, Phys. Rev. D **51**, 3237 (1995).
[53] F.J. Klein, Ph.D. thesis, Bonn University, 1996; SAPHIR Collaboration, F.J. Klein *et al.*, πN Newslett. **14**, 141 (1998).

[54] CLAS Collaboration, M. Battaglieri *et al.*, Phys. Rev. Lett. **90**, 022002 (2003).
[55] Y. Oh and T.-S.H. Lee, Phys. Rev. C **66**, 045201 (2002).
[56] A. Sibirtsev and W. Cassing, Eur. Phys. J. A **7**, 407 (2000).
[57] J. Ballam *et al.*, Phys. Rev. D **7**, 3150 (1973).
[58] D.P. Barber *et al.*, Z. Phys. C **12**, 1 (1982).
[59] CLAS Collaboration, E. Anciant *et al.*, Phys. Rev. Lett. **85**, 4682 (2000).
[60] D.J. Tedeschi, in *Proceedings of the International Symposium on Electromagnetic Interactions in Nuclear and Hadron Physics, Osaka, 2001*, edited by M. Fujiwara and T. Shima (World Scientific, Singapore, 2002), p. 367.
[61] T. Nakano, *Proceedings of the International Symposium on Electromagnetic Interactions in Nuclear and Hadron Physics, Osaka, 2001* (World Scientific, Singapore, 2002), p. 24.
[62] A.I. Titov, M. Fujiwara, and T.-S.H. Lee, Phys. Rev. C **66**, 022202(R) (2002).
[63] H.J. Besch, G. Hartmann, R. Kose, F. Krautschneider, W. Paul, and U. Trinks, Nucl. Phys. **B70**, 257 (1974).